HHS Public Access

Author manuscript

Nat Cancer. Author manuscript; available in PMC 2022 November 26.

Published in final edited form as:

Nat Cancer. 2022 June ; 3(6): 734–752. doi:10.1038/s43018-022-00375-0.

Breast cancer patient-derived organoid screening implicates the repressor NCOR2 in cytotoxic stress response and anti-tumor immunity

Kelvin K. Tsai[1,2,3,4,7,8], **Shenq-Shyang Huang**[3,7], **Jason J. Northey**[1], **Wen-Ying Liao**[3], **Chung-Chi Hsu**[3], **Li-Hsin Cheng**[3], **Michael E. Werner**[1], **Chih-Pin Chuu**[5], **Chandrima Chatterjee**[6], **Jonathan N. Lakins**[1,6], **Valerie M. Weaver**[*,1,2,6,8]

[1]Department of Surgery and Center for Bioengineering and Tissue Regeneration, University of California, San Francisco, San Francisco, CA 94143, USA

[2]Department of Radiation Oncology, Department of Bioengineering and Therapeutic Sciences, Eli and Edythe Broad Center of Regeneration Medicine and Stem Cell Research, Helen Diller Family Comprehensive Cancer Center, University of California San Francisco, San Francisco, CA 94143, USA

[3]Laboratory of Advanced Molecular Therapeutics, Graduate Institute of Clinical Medicine, College of Medicine, Taipei Medical University, Taipei, 110301, Taiwan

[4]Department of Medicine, Wan Fang Hospital, Taipei Medical University, Taipei, 116079, Taiwan

[5]Institute of Cellular and System Medicine, National Health Research Institutes (NHRIs), Miaoli, 350401, Taiwan

[6]Department of Pathology and Institute for Medicine and Engineering, University of Pennsylvania, Philadelphia, PA 19104, USA

[7]These authors contributed equally

[8]These authors jointly supervised this work

[*]Correspondence: Valerie M. Weaver, Ph.D., University of California, San Francisco, 513 Parnassus Avenue, 565 Health Sciences East, San Francisco, CA 94143-0456, Valerie.weaver@ucsf.edu Telephone: 415-476-3973, Kelvin K. Tsai, M.D., Ph.D., Graduate Institute of Clinical Medicine, College of Medicine, Taipei Medical University, 7F, 250 Wuxing St., Xinyi Dist., Taipei City 11031, Taiwan, tsaik@tmu.edu.tw Telephone: +886 2-2736-1661.

Author contributions

V.M.W. conceived the original concept and acquired provisional funding and directed the proof-of-concept studies which were executed by C.C. and J.N.L. Thereafter V.M.W. and K.K.T. acquired sustained funding to execute the studies and together designed and directed the investigative work. K.K.T. conceptualized the DeCOR2 gene therapy and acquired funding to support proof-of-concept work. K.K.T., J.N., S-S.H., C-C.H., L-H.C., M.W., S.K. and J.N.L. conducted the molecular, biochemical, and functional studies. C-P.C. carried out the MWA analysis. S-S.H. and C-C.H. performed immunohistochemistry analyses. K.K.T. analyzed the microarray data, directed the bioinformatics analysis, performed clinical correlative analysis. J.N. and S-S.H. completed patient derived organoid studies. S-S.H., W-Y.L. and J.N. conducted animal work. K.K.T. and V.M.W. co supervised the studies and data analysis and together summarized and interpreted data and co-wrote the manuscript with input from coauthors.

Competing Interests

K.K.T. is the named inventor on a U.S. provisional patent application (application number 63302570). The remaining authors declare no competing interests.

Supplementary Information is available for this paper.

Abstract

Resistance to anti-tumor treatment contributes to patient mortality. Functional proteomic screening of chemotherapy-treated breast cancer patient-derived organoids (PDOs) identified nuclear co-repressor-2 (NCOR2) histone deacetylase as an inhibitor of cytotoxic stress response and anti-tumor immunity. High NCOR2 in the tumors of breast cancer patients predicted chemotherapy refractoriness, tumor recurrence and poor prognosis. Molecular studies revealed NCOR2 inhibits anti-tumor treatment by regulating histone deacetylase-3 (HDAC3) to repress IRF1-dependent gene expression and interferon (IFN) signaling. Reducing NCOR2 or impeding its epigenetic activity by modifying its interaction with HDAC3 enhanced chemotherapy responsiveness and restored anti-tumor immunity. An adeno-associated viral NCOR2-HDAC3 competitor potentiated chemo-, and immune checkpoint therapy in culture and in vivo by permitting transcription of IRF1-regulated pro-apoptosis and inflammatory genes to increase IFNγ signaling. The findings illustrate the utility of PDOs for drug discovery, and suggest targeting stress and inflammatory-repressor complexes such as NCOR2/HDAC3 could overcome treatment resistance and improve cancer patient outcome.

INTRODUCTION

Therapy resistance limits the efficacy of anti-neoplastic treatment and is the major cause of patient mortality[1]. Despite advances in understanding how apoptosis and autophagy is executed at the cellular level[2,3], experimental findings clarifying the molecular basis of therapy resistance[4], and innovative immune therapies[5–8], treatment resistance in cancer patients remains a major clinical challenge.

Therapeutic resistance in tumors may be due to the selective outgrowth of cancer cells with genetic alterations that enhance their growth and survival, or intrinsically death-resistant stem-like tumor cells[4,9]. Regardless, treatment efficacy depends upon stimulation of anti-tumor inflammation and efficient T cell killing of tumor cells. Thus, therapy resistance in tumors could arise because cancers cultivate a pro-tumor inflammatory response, develop compromised T cell killing, or fail to recruit and support anti-tumor CD8 T cells[6,7,10]. Exposure of tumors to cytotoxic agents and ionizing radiation creates ligands that activate nucleic acid-sensing Toll-like receptor (TLRs), cGAS-STING, and RIG-I/MAVs pathways, leading to Type I Interferon (IFN) production that is critical for anti-tumor immunity, regardless of tumor cell genotype or stem-like phenotype[11,12]. Accordingly, compromised TLR-induced IFN responsiveness could underlie the origin of some therapy resistant tumors.

Treatment-triggered IFN secretion directly inhibits tumor cell proliferation and induces apoptosis[11,13], and activates an anti-tumor immune response[10]. Dysregulation of IFN signaling is one mechanism viruses and some tumors use to evade immune attack and to avoid cell death[7]. This mechanism can encompass deletion of type-1 IFN genes and/or defects in IFN receptors and their downstream signaling molecules such as IFN response factors, IRF1 and 7[13,14]. Optimal physiological response to infection, injury or disease entails a tightly regulated balance between pro-inflammatory and anti-inflammatory responses that rely upon intrinsic mechanisms to prevent induction of a life-threatening cytokine storm[15]. These IFN-linked regulatory circuits include anti-inflammatory proteins

such as suppressor of cytokine signaling (SOCS) and checkpoint receptors that dampen signaling to prevent hyper activation of stress response signaling[16,17]. Consistently, treatment resistance in some tumors derives from increased expression and activity of checkpoint receptors that can significantly compromise anti-tumor immunity[18]. Some normal cells express transcriptional regulatory mechanisms that repress IFN signaling to regulate developmental processes such as positive and negative T cell maturation[19]. This suggests that tumors could exploit similar regulatory molecules to restrict their IFN-dependent anti-inflammatory response, as reported for the PBAF form of the SWI/SNF chromatin remodeling complex in melanoma[8]. It follows, tumors with a tempered IFN-dependent anti-inflammatory transcriptional response would be able to thwart stress-induced activation of Toll-like receptor-dependent death to acquire resistance to a spectrum of cancer therapies including chemotherapies and anti-tumor immunity. Identifying molecules that regulate IFN-dependent signaling could identify new anti-tumor drug targets and to overcome the treatment resistance in some cancers.

We sought to identify molecules intrinsically upregulated in tumors that temper cytotoxic stress-induced and pro-inflammatory transcriptional programs, and to causally implicate these candidates in the anti-tumor treatment resistance phenotype observed in cancer patients. To accomplish this, we exploited breast cancer patient-derived organoids (PDOs) that were previously established from patient-derived triple negative breast cancer (TNBC) xenografts (PDXs), that exhibited increasing levels of intrinsic resistance to cytotoxic stress[20]. Chromatin immunoprecipitation (IP) screens identified nuclear receptor co-repressor 2 (NCOR2) as a transcriptional repressor scaffold highly expressed in the treatment resistant PDOs. NCOR2 was shown to confer resistance to cytotoxic stress-induced apoptosis in breast cancers by repressing IRF1-dependent transcription to reduce anti-tumor immunity[21,22]. The findings were validated in PDXs, immortalized breast cancer cells, syngeneic models, patient biopsies and clinical data sets. The efficacy of an adenoviral NCOR2-histone deacetylase 3 competitor, the Decoy of NCOR2 (DeCOR2), to potentiate chemo-, and immune-therapy in preclinical murine and PDX avatar models was demonstrated through its ability to permit transcription of IRF1-regulated pro-apoptosis and anti-tumor immune modulatory genes. The discovery underscores the power of using PDOs for anti-tumor drug studies. Targeting conserved nuclear scaffolds that regulate stress and inflammatory transcriptional repressor hubs is a potential approach to overcome treatment resistance and improve cancer patient outcome.

RESULTS

Organoid screening implicates IRF1 in tumor treatment response

PDOs have been used to examine the therapy responsiveness of patient tumors and to identify new anti-cancer treatments[22–25]. We obtained three independent PDOs: HCI-001, HCI-002 and BCM-2665 established from distinct TNBC PDXs exhibiting varying degrees of resistance to cytotoxic agents[22,25]. We treated the resistant PDO HCI-001 with increasing doses of the chemotherapeutic (C/T) agents paclitaxel and doxorubicin and the death receptor ligand TNF-related apoptosis inducing ligand (TRAIL), and compared the percent cell death induction to that exhibited by the moderately BCM-2665[22] and

more sensitive HCI-002 PDOs (Fig. 1a,b). To identify molecular pathways that could modulate the differential treatment responsiveness, we performed RNA sequencing (RNA-seq) on paclitaxel pre and post treated PDOs. IRF1 was identified as the top-ranked apoptosis-regulatory gene that was the most strongly upregulated in the chemo-sensitive PDOs (HCI-002) as compared to the chemo-resistant PDOs (HCI-001) (Fig. 1c). Gene profiling of several immortalized breast cancer cell lines representing diverse breast cancer subtypes similarly revealed IRF1 to be highly induced by C/T in the treatment sensitive cells (Extended Data Fig. 1a–d). Promoter analysis revealed the consensus binding site of IRF1, the interferon regulator factor element (IRF-E), was enriched amongst the induced PCD genes, and that this promoter element comprised 28 percent of the PCD genes induced by C/T (Extended Data Fig. 1c, lower panel; Extended Data Fig. 1e). Death sensitivity of the PDOs to paclitaxel correlated with the level of IRF1 mRNA induced (HCI-002, BMC-2665 and HCI-001; Fig. 1d). Functional relevance of IRF1 induction to the chemosensitivity of the PDOs was illustrated by showing that knockdown (KD) of *IRF1* expression, using two independent short-hairpin RNAs (shRNA), reduced the percent cell death induced by C/T (paclitaxel/doxorubicin) in the most sensitive HCI-002 PDOs (Fig. 1e,f). The HCI-002 PDOs lacking IRF1 expression were also highly resistant to TRAIL, which is a treatment that induces apoptosis independent of cell proliferation (Fig. 1f)[26]. *IRF1* knockdown compromised the ability of C/T treatment to shrink xenografted organoids generated from immortalized TNBC breast cancer cells (Extended Data Fig. 1i). The studies identified IRF1, a highly conserved pro-apoptosis and pro-inflammatory transcription factor[27–29], as a key regulator of treatment response in human breast cancer PDOs and immortalized breast cancer cells. Because PDOs recapitulate many of the intrinsic therapy responsiveness observed in cancer patients[21], the data implicate IRF1 and factors modulating its activity in the treatment resistance phenotype of human breast cancers.

Proteomic screening identifies NCOR2 as a cell death inhibitor

Correlative analysis of clinical data from neoadjuvant C/T treated breast cancer patients failed to reveal any consistent relationship between IRF1 expression and treatment response (Supplementary Table 2). Therefore, we sought to identify molecules interacting with IRF1 that could modify its transcriptional activity. We compiled a list of 461 GO-annotated chromatin and epigenetic regulating proteins. We then used co-immunoprecipitation (IP) followed by a high-throughput robotic Micro-Western Array (MWA) screening platform to identify proteins that strongly associated with IRF1 following cell death stimulation (Fig. 1g)[30]. We used immortalized HMT-3522 T4–2 cells which represent an early-transformed, basal-like breast cancer cell line that strongly upregulated IRF1 following C/T treatment (Extended Data Fig. 1c, upper panel). To uncouple cell growth and IRF1-dependent apoptosis sensitivity we also induced cell death using TRAIL. The screen identified several histone methyl transferases, demethylases, chromatin remodeling factors, and transcriptional co-activators that bound specifically to a nuclear IRF1 complex (Supplementary Table 3). An IRF1 binding index identified the transcriptional activator lysine methyltransferase 2C (KMT2C; *MLL3*) and the histone hypoacetylation and chromatin remodeling transcriptional repressor, nuclear receptor co-repressor 2 (NCOR2; *NCOR2*) as the two highest ranked nuclear bound IRF1 proteins (Fig. 1h)[31,32]. Immunofluorescence staining revealed that the most treatment-resistant HCI-001 PDOs also had the highest expression of NCOR2

(Fig. 1i). The chromatin repressor NCOR2 modulates STAT1 dependent gene transcription to restrict viral-stimulated inflammatory response in macrophages[33]. Thus, we reasoned that the treatment resistance exhibited by the HCI-001 PDOs could be linked to NCOR2-mediated *IRF1* transcriptional repression. Consistently, co-IP revealed that NCOR2, but not its paralog nuclear co-repressor (*NCOR1*), interacted with endogenous IRF1 in the nuclear lysates of primary human breast cancer cells and in assorted immortalized breast cancer cells (Fig. 1j,k; Extended Data Fig. 2a). The domains within IRF1 that mediate its binding to NCOR2 were mapped to its N-terminal region (amino acid 1–89; Fig. 1l; Extended Data Fig. 2b,c). Functional studies showed that forced overexpression of the NCOR2-binding region (NBD) of IRF1 abrogated IRF1-NCOR2 binding (Fig. 1m). The IRF1-binding region on NCOR2 was mapped to its extreme C-terminal region (amino acid 2079–2514; Fig. 1n,o; Extended Data Fig. 2d–f) confirmed by showing that a C-terminus-deleted mutant of NCOR2 failed to interact with IRF1 (Fig. 1p; Extended Data Fig. 2g). The findings identify the transcriptional repressor NCOR2 as a chromatin scaffolding protein whose interaction with IRF1 is stimulated by exposure to a cytotoxic stress. The results further suggest that NCOR2 could prevent cell death induction in response to C/T by directly binding to IRF1 to inhibit its transcriptional activity.

NCOR2 inhibits IRF1 transcription to drive treatment resistance

We next asked if NCOR2 could modulate the treatment-resistant phenotype of PDOs and breast cancer spheroids via its ability to bind and inhibit IRF1s transcriptional activity. We knocked down *NCOR2* in the C/T-resistant TNBC PDO HCI-001 and basal-like HMT-3522 T4–2 cells using lentivirus-mediated expression of shRNA (Figure 2a; Extended Data Fig. 3a). Knockdown (KD) of *NCOR2* expression significantly enhanced the transcriptional activity of IRF1 (Extended Data Fig. 3b). We then assayed the cell death sensitivity of the PDOs and spheroids (diameter ~100 μm) embedded within recombinant basement membrane (rBM) to C/T agents and TRAIL. *NCOR2* KD sensitized the HCI-001 PDOs and the HMT-3522 T4–2 spheroids to paclitaxel, doxorubicin and TRAIL (Figure 2b; Extended Data Fig. 3c). KD of *NCOR2* expression also sensitized breast cancer spheroids generated using luminal and $HER2^+$ molecular subtype immortalized cell lines and pancreatic cancer spheroids to C/T drugs, TRAIL, and ionizing radiation (Extended Data Fig. 3d–f). To determine if NCOR2 could enhance resistance to cytotoxic stress-induced apoptosis, we treated immortalized human breast cancer cells engineered to overexpress NCOR2 with cell death stimuli and assayed spheroids for their apoptosis sensitivity to C/T agents and TRAIL treatment. TNBC MDA-MB-231 human breast cancer spheroids overexpressing NCOR2 were highly resistant to cytotoxic stress-induced apoptosis (Fig. 2c,d; Extended Data Fig. 3g). However, when both NCOR2 and/or IRF1 were co-expressed, the full-length NCOR2 overrode the cell death stimulated by overexpression of IRF1 or STAT1 (Fig. 2e). Similarly, over expression of the NBD of IRF1 not only abrogated IRF1-NCOR2 binding (Fig. 1m), but also sensitized the treatment-resistant HCI-001 PDOs as well as primary breast cancer NHRI-BC-008 cells to C/T (Fig. 1q). Expression of an IRF1-binding-domain (IBD)-deficient mutant of NCOR2 (prevents IRF1 interactions; Fig. 1n,p) sensitized the breast cancer cells to TRAIL stimulated cell death (Fig. 2f). The findings implicate NCOR2 in modulating the death sensitivity phenotype of human breast PDOs and immortalized

breast tumor cells, and indicate that this effect is mediated through its ability to interact with IRF1.

We next implanted immortalized human breast cancer cells engineered to express high *versus* low levels of NCOR2 into the mammary fat pads of immune compromised NOD-SCID mice or into the flanks of nude mice and treated the animals with C/T agents. The mouse studies revealed that the tumors generated by the breast cancer cells that expressed high NCOR2 were nonresponsive to either doxorubicin (Fig. 2g) or paclitaxel (Fig. 2h) with minimal induction of apoptosis, as revealed by low levels of cleaved caspase-3 (Fig. 2i). The mice harboring NCOR2^{high} tumors also exhibited reduced overall survival (Fig. 2j). The data are consistent with a causal role for NCOR2 in modulating C/T agents, IR and TRAIL-induced apoptosis in tumors. The findings suggest that NCOR2 can prevent cell death induced in response to C/T and immune receptor activator ligation by directly binding to IRF1.

NCOR2 expression correlates with therapy resistance in cancer patients

By interrogating the transcript level of *NCOR2* in multiple cohorts of neoadjuvant-treated breast cancer patients (total $n = 217$)[34–36], we noted that tumors with overall higher NCOR2 expression had a substantially greater (up to 13.6-fold; $P = 0.004$) odds ratio of treatment unresponsiveness compared with tumors with lower *NCOR2* expression (Fig. 3a; Supplementary Table 4). Analysis revealed that less than 4% of the NCOR2^{high} tumors responded to systemic C/T (Fig. 3b). Multivariate analysis confirmed that *NCOR2* expression is a strong predictor of therapeutic resistance (odds ratio = 17.142; $P = 0.019$) independent of clinical-pathological criteria and the molecular subtypes of breast cancer (Supplementary Table 5). By contrast, the baseline expression levels of the NCOR2 paralog *NCOR1* or the other components in the NCOR2 corepressor complex, including *HDAC3* and *IRF1*, had no prognostic value (not shown).

NCOR2 is not only a robust predictor of therapeutic response in the neoadjuvant setting but can also predict long-term outcome in the adjuvant setting. In a cohort of 295 breast cancer patients who had received surgery[37], the *NCOR2* transcript levels inversely correlated with overall or relapse-free survival only in those patients who had received adjuvant systemic C/T, but not in those who did not receive C/T (Fig. 3c,d). Findings were confirmed in a meta-analysis encompassing 13 independent cohorts of breast cancer patients ($n = 1586$; Fig. 3e,f)[38]. In a Cox model, the *NCOR2* expression level interacted significantly with patients' adjuvant C/T status ($P = 0.007$), and was a strong and an independent predictor of survival and disease relapse in C/T-treated patients (hazard ratio for death = 9.64, $P < 0.001$; Supplementary Table 6). We noted that the expression level of *NCOR2* only marginally varied among different molecular subtypes and its prognostic value superseded that of the molecular subtypes across independent patient cohorts (Supplementary Tables 6 and 7).

Nuclear NCOR2 confers treatment resistance to breast cancer cells

To clarify NCOR2 molecular activation following C/T stress exposure we analyzed biopsies of neoadjuvant-treated human breast cancer patient tissue, whose incomplete pathological response associates with poorer overall survival and enhanced rate of tumor recurrence[39].

Immunohistochemistry analysis of human breast tumor biopsies from these treated patients revealed that there was enhanced intensity of nuclear NCOR2 staining in the residual, C/T-resistant tumors (Fig. 3g). We also quantified an increase in nuclear NCOR2 in cultured PDOs, breast cancer cell spheroids and xenografted breast cancer cell tissue treated with paclitaxel or TRAIL (Fig. 1j; Extended Data Fig. 4a,b). Impeding the nuclear translocation of NCOR2, by expressing a functionally deficient RanGTPase mutant or a mutant NCOR2 lacking its nuclear localization signal (NLS), sensitized breast cancer cells to apoptosis induction (Extended Data Fig. 4c–g). Thus, NCOR2 likely mediates its treatment resistance through its gene repressor activity whose scaffolding function depends upon its nuclear localization.

NCOR2 represses IRF1-dependent apoptosis through HDAC3

NCOR2 represses gene transcription by altering histone hypoacetylation[31,32] through the recruitment and activation of HDACs[40]. Treatment of breast tumor cells engineered to express high levels of NCOR2 with general HDAC inhibitors sensitized the cells to cytotoxic stress (Fig. 4a). HDAC3 is the predominant deacetylase binding partner of NCOR2 in mammalian cells[32,41] that we confirmed through co-IP assays in nuclear lysates from TRAIL-treated HMT-3522 T4–2 cells (Fig. 4b). We found that shRNA-mediated knockdown of *HDAC3* expression (Fig. 4c) re-sensitized breast cancer cells overexpressing NCOR2 to cytotoxic stress induced cell death (Fig. 4d) and restored cytotoxic stress-induced IRF1 transcriptional activity (Fig. 4e). We therefore tested whether the HDAC3-NCOR2 interaction mediates the death resistance phenotype by stably expressing a functionally-compromised mutant of NCOR2, NCOR2 (K449A), which binds HDAC3 and prevents its deacetylase activity (Fig. 4f)[31], in the HMT-3522 T4–2 cells, and assayed for sensitivity to cell death induction. We verified that the mutant NCOR2 was competent to interact with HDAC3 and prevented its nuclear deacetylase activity (Fig. 4f), and thereafter assessed its ability to regulate cell death resistance. NCOR2 (K449A) expression hyper-sensitized the breast cancer cells to TRAIL-induced apoptosis (Fig. 4g). Thus, NCOR2 collaborates with HDAC3 to repress IRF1-/STAT1-dependent transcription likely through regulating promoter accessibility. The data further suggest that this repressor function promotes treatment resistance in breast cancer cells by preventing pro-stress gene expression (Fig. 4h).

NCOR2 represses IRF1-dependent cell death transcription

We next profiled gene expression in breast cancer spheroids that expressed either an empty vector or that over expressed NCOR2 and that were treated with either vehicle or the cell death receptor ligand TRAIL (Fig. 5a). We identified and then focused our assessment on a list of 64 genes related to programmed cell death (PCD) whose induced or repressed differential expression was regulated by NCOR2 (Supplementary Table 8; Fig. 5b). Analysis revealed that the majority of the PCD genes differentially regulated by NCOR2 were less robustly induced following TRAIL treatment. *In silico* promoter examination confirmed that the majority (n = 47; 73.4%) of these PCD genes contained the IRF-E and/or the STAT1-binding sites in their promoters (Fig. 5b, yellow boxes). Whereas IRF1 promotes apoptosis by inducing transcription of apoptosis regulating molecules including TRAIL[28], caspase-1, -7, and -[29,42], analysis revealed that breast cancer cells expressing high levels of NCOR2 failed to increase expression of *TNFSF10*, *CASP7*, *CASP1* or *IRF1* following treatment

with either TRAIL or C/T agents (Fig. 5c; Extended Data Fig. 5). We also determined that breast cancer cells expressing high levels of NCOR2 (K449A), which binds HDAC3 and prevents its deacetylase activity (Fig. 4f), did not repress the expression of these same genes (Fig. 5d). Chromatin immunoprecipitation (ChIP) PCR and ChIP-re-ChIP assays confirmed the co-recruitment of NCOR2 and HDAC3 to the IRF-E on the promoter regions of the targeted PCD genes, and did so in tandem with histone deacetylation, while simultaneously attenuating recruitment of transcription factor IIB (TF IIB) and RNA polymerase II (Pol II; Fig. 5e; Extended Data Fig. 6a). Further analysis revealed that in cytotoxic stimuli (TRAIL)-treated HMT-3522 T4–2 cells, NCOR2 also recruited STAT1 into the complex with HDAC3, TFIIB and Pol II (Fig. 5f; Extended Data Fig. 6b). Findings revealed that NCOR2 is recruited to the promoter regions of *TNFSF10*, *CASP1, CASP7*, and *STAT1* where studies suggested their histone hypoacetylation and transcriptional repression was induced (Fig. 5e; Extended Data Fig. 6c). Knockdown of *NCOR2* expression reduced the recruitment of HDAC3 to the promoters of the PCD genes we examined, leading to histone hyperacetylation and transcriptional activation (Extended Data Fig. 6d). Thus, cancer cells could acquire treatment resistance by promoting the nuclear localization of NCOR2. The findings suggest that nuclear localized NCOR2 assembles into a complex with STAT1/IRF1 and HDAC3 to repress “stress signaling responsiveness” by regulating promoter accessibility to inhibit the expression of PCD and stress genes that reduce cell death induction (Fig. 5g).

Inhibiting NCOR2-HDAC3 function sensitizes breast tumors to treatment

We next designed a therapeutic strategy to ablate NCOR2’s HDAC3 function. We constructed a small (306 amino acid; ~35.9 kDa) protein termed “Decoy of NCOR2” or “DeCOR2” that consists of the deacetylase-activating domain and the NLS of NCOR2 (Fig. 6a). DeCOR2 was designed to compete with endogenous NCOR2 to prevent its association with HDAC3 and inhibit its ability to recruit IRF1, and/or other stress response transcriptional regulators (Fig. 6b,c). When stably expressed in breast cancer cells, DeCOR2 enhanced baseline and cytotoxic stimuli-induced transcriptional activity of IRF1 (Fig. 6d), and permitted cell death induction in breast cancer cells in response to C/T agents and TRAIL, regardless of endogenous NCOR2 levels (Fig. 6e). Deleting the NLS from DeCOR2 completely abolished its ability to sensitize breast cancer cells to cytotoxic stress (DeCOR2 (ΔNLS); Fig. 6f), whereas replacing the endogenous NLS with a strong triplicated NLS derived from SV40 large T (LT) antigen potentiated its activity (DeCOR2 (3×LT-NLS); Fig. 6f).

We constructed a potent adeno-associated virus (AAV) vector, which is considered a safe and clinically feasible system for therapeutic gene delivery in solid cancers[43], which carries a DeCOR2-expression cassette whose small size enables its incorporation into the majority of viral DNA backbones. Infection with DeCOR2 packaged with a recombinant and chimeric AAV vector (AAV-DJ)[44] sensitized breast cancer spheroids to cytotoxic stress (Fig. 6g). To optimize the AAV-DJ-DeCOR2 therapy, we administered the viruses into mice harboring established orthotopic breast tumors and verified the expression of DeCOR2 in the tumor (Fig. 6h). Four days following the AAV infection, the tumors were treated with paclitaxel using a clinically relevant regimen (Fig. 6i). The AAV-DJ-DeCOR2 gene therapy rendered the tumors highly sensitive to paclitaxel treatment, whereas the control-

AAV-infected tumors remained resistant (Fig. 6j). The AAV-DJ-DeCOR2 gene therapy also sensitized established orthotopic PDX TNBC tumors (Fig. 6k), that expressed moderate-to-high levels of NCOR2 (Fig. 6l), to C/T, ultimately stabilizing the disease (Fig. 6m). We noted that the PDX tumors receiving the AAV-DJ-DeCOR2/paclitaxel combination therapy contained more apoptotic cells than those receiving C/T alone (Fig. 6n). The findings validate the application of this anti-tumor treatment, and demonstrate its ability to sensitize experimental and PDX tumors with high NCOR2 to a clinically relevant regime of C/T.

Inhibiting NCOR2-HDAC3 function enhances anti-tumor immunity

NCOR2 can reduce inflammatory gene expression and thus may have the potential to modulate anti-tumor immunity[10]. Using a syngeneic model of TNBC, 4T1 murine breast tumor cells that expressed high levels of NCOR2 (Fig. 7a), transcripts levels of the T-cell chemokines CCL4, CXCL9, CXCL10, IL6, IFNγ, the immune checkpoint molecule programmed death ligand 1 (PDL1; *CD274*), and TRAIL (*TNFSF10*), were induced when murine *NCOR2* (m*NCOR2*) was knocked down (Fig. 7b,c). Protein levels of CXCL9, IL6, and IFNγ were also elevated in the *mNCOR2* knockdown 4T1 cells (Fig. 7d). Knockdown of m*NCOR2* in the 4T1 breast tumor cells was accompanied by elevated IFNγ transcriptional activity (Fig. 7e). m*NCOR2*-deficient 4T1 breast tumor cells were also more responsive to IFNγ, as indicated by higher expression of IFNγ pathway genes, including *CXCL10*, *IFIT1*, *IFIT2*, and *IFIT3* (Fig. 7f)[6], and the cells were more sensitive to IFNγ-induced death (Fig. 7g). 4T1 breast tumor cells engineered to express murine DeCOR2 (mDeCOR2), using an inducible promoter, showed an early reduction in tumor growth in syngeneic mice, whereas this effect was greatly abrogated when the tumors were implanted into recombination activating 1 (*RAG1*) genetic knockout mice ($RAG1^{-/-}$; a mouse model that lacks functional lymphocytes; Fig. 7h, left). The breast tumors formed in the *RAG1* knockout mice were also less responsive to C/T than the treated tumors implanted into syngeneic host mice (Fig. 7h, right). When treated with the AAV-DJ-mDeCOR2 gene therapy, the 4T1 breast tumors had increased infiltration of $CD8^+$ tumor-infiltrating lymphocytes (TILs). The treated tumors also had higher numbers of activated IFNγ and tumor necrosis factor-alpha (TNF-α) TILs, and a higher ratio of $CD8^+$ effector T cells to forkhead box protein P3 $(FoxP3)^+$ regulatory T cells; indicating restoration of a functional anti-tumor response (Fig. 7i)[45]. This anti-tumor immune response was accompanied by a heightened apoptosis sensitivity to treatment with C/T agents and IFN-γ (Fig. 7j). Thus, by permitting the transcription and release of chemokines related to the recruitment and expansion of anti-tumor T cells and/or dendritic cells, abrogating NCOR2-HDAC3 function in breast tumors can potentiate anti-tumor immunity.

A phase III clinical trial demonstrated a higher percentage of a pathological complete response in patients with early stage TNBC treated with the programmed death 1 (PD1) antibody pembrolizumab, resulting in its accelerated clinical approval, underscoring the potential for immune checkpoint inhibitors (ICIs) to treat breast cancer[,46]. A T-cell inflamed microenvironment characterized by active IFNγ and IRF1 signaling, and high levels of TIL infiltration predicts the responsiveness of tumors to immune checkpoint inhibitors[5,47]. We showed that either knocking down or disabling NCOR2's HDAC3 activity in breast tumors facilitated their IFNγ signaling activity, fostered an immunogenic microenvironment

(Fig. 7c), and increased the percentage of PD-L1-expressing cells in the tumors (5.8-fold increase; Fig. 8a). We posited that disabling the NCOR2/HDAC3 complex, by treating the cells with DeCOR2, could potentiate the anti-tumor efficacy of ICIs. Although treatment of 4T1 breast tumors, which express a high level of NCOR2 (Fig. 7a), with anti-mouse PD1 (mPD1) antibody alone only modestly reduced tumor enlargement, combination therapy with AAV-DJ-mDeCOR2 and anti-mPD1 antibody significantly retarded tumor expansion and concomitantly induced extensive apoptosis (Fig. 8b–d). Whilst the AAV-DJ-DeCOR2 therapy enhanced the infiltration and activity of effector $CD8^+$ T cells within the tumors ($IFN\gamma^+$; Fig. 8e), the combination therapy greatly potentiated the anti-tumor immune response to a much greater extent than that induced by the AAV-DJ-DeCOR2 therapy or the anti-mPD1 therapy alone (Fig. 8f,g). To explore if the mDeCOR2 therapy could induce lasting immune memory that could enhance ICI responsiveness in secondary tumors not directly administered the gene therapy, we treated 4T1 breast tumors with neoadjuvant AAV-DJ-mDeCoR2, surgically excised the tumors, and then re-challenged the mice through establishing tumors on the contralateral mammary fat pad (Fig. 8h). The neoadjuvant mDeCOR2 therapy rendered the secondary tumors hypersensitive to anti-mPD1 antibody, whereas those mice that did not receive the mDeCOR2 therapy in their primary tumors barely responded to the ICI therapy (Fig. 8i,j). The results suggest that in addition to its ability to repress C/T and cell death receptor ligand-mediated death, NCOR2 additionally influences anti-tumor immunity.

Conclusions

We discovered that human breast tumors can engage the chromatin repressor NCOR2 to ameliorate their responsiveness to C/T, cell death receptor, radiation, and immune-stimulated cell death. Our studies revealed that NCOR2 associates with HDAC3 and assembles into a chromatin-binding complex with STAT1 to inhibit the anti-tumor treatment responsiveness of breast cancers to repress the transcription of cell death and inflammatory genes induced by IRF1. Our findings are consistent with prior studies showing tumors with mutations or deletions in molecules that regulate IFN-γ signaling compromise treatment and limit anti-tumor immunity in experimental tumor models and cancer patients[6,7]. Our discovery expands this paradigm to include conserved regulatory mechanisms that modulate pro-inflammatory and pro-stress signaling to temper tumor treatment response, as has been observed in macrophages that can develop tolerance to sustained Toll-like receptor stimulation through the NFκB repressosome[48]. A similar transcriptional repressor phenotype was reported for the SWI/SNF PBAF complex that represses inflammation to limit checkpoint inhibitor responsiveness in melanoma[49], and in macrophages that exploit nuclear NCOR (*NCOR1*) to repress IRF7 to restrain over activation of the antiviral response[33]. Unlike these examples, we discovered a nuclear scaffold that regulates the expression of a suite of genes that regulate stress and inflammatory signaling and showed this mechanism also limits the feedforward signaling that amplifies treatment response and regulates anti-tumor immunity. This phenotype is analogous to the histone deacetylase HDAC3 mechanism used by intestinal epithelial cells to curtail the inflammation induced by commensal-bacteria- or chemical-induced damage[50]. While we studied breast tumors, this repressor mechanism appears to be conserved in other tumor types (unpublished findings)

suggesting targeting conserved stress- and inflammatory-repressor checkpoints such as NCOR2 comprises a broad approach to overcome resistance to cytotoxic stress and T cell immune treatment.

Many solid human tumors are intrinsically resistant to anti-cancer therapy, which limits the efficacy of anti-neoplastic treatment and is the major cause of patient mortality[4]. Preoperative neoadjuvant C/T decimates the primary tumor in less than 10% of ER-positive breast tumors and 20–30% of ER-negative tumors[51]. Approximately 30% of breast cancer micrometastases following surgery are sensitive to adjuvant C/T. Despite recent advances in cancer immunotherapy, clinical studies demonstrate that only a minority (less than 20%) of cancer patients benefit from the therapy[52]. Our finding that NCOR2 expression and nuclear activity is strongly linked to the therapeutic outcome of primary breast tumors implies that the pleiotropic and multi-drug resistance phenotype of tumors may be acquired at an early stage of tumor development, possibly prior to therapy. Most HDAC inhibitors, which can be quite toxic, target multiple classes of HDAC and have been clinically disappointing, with the exception of benzamide HDAC inhibitor for the treatment of hormone-receptor-positive breast cancer,[53]. By contrast, DeCOR2 gene therapy selectively disrupts the NCOR2-HDAC3 stress-repressor complex and sensitizes tumor cells to systemic C/T and at least one immunotherapy. Accordingly, the DeCOR2 gene therapy may be amenable to different clinical scenarios either before, concomitant with, or after C/T or immunotherapy.

PDOs have emerged as attractive models to recapitulate architectural and genomic characteristics of the primary tumor and to reflect and predict the responsiveness of the primary tumor[54–56]. We exploited PDOs established from PDXs and breast cancer cell spheroids for C/T[57,58], death receptor ligation and IR studies to capture the conserved molecular signals associated with resistance to cell death stimuli. We illustrated the utility of PDOs and spheroids by identifying NCOR2 as a key regulator of treatment resistance through its ability to repress pro-death/pro-inflammatory gene expression. Although NCOR2 can directly regulate DNA repair in specific instances, our studies suggest that NCOR2's predominantly influences treatment responiveness via its ability to regulate the transcription of pro-inflammatory and pro-stress genes. We observed a similar induction of γH2AX and Nijmegen Breakage Syndrome Protein 1 (NBS1; representing DNA double strand break), up regulation of genes implicated in DNA-damage-induced p53 activation and double strand break repair, and increased expression of genes related to the DNA damage response following chemotherapy treatment, irrespective of whether or not the cells expressed NCOR2 (Extended Data Fig. 3h–j; Extended Data Fig. 7a–c). Whereas knockdown of *RAD50* compromised DNA damage repair signaling and enhanced cytotoxic death induction following chemotherapy treatment, *RAD50* knockdown cells could be rescued by overexpression of NCOR2 (Extended Data Fig. 7d–f). Although NCOR2-HDAC interactions modulates chromatin organization and stress/inflammatory gene expression, we found no convincing evidence NCOR2 globally modulated chromatin organization or methylation (similar levels of nuclear acetylated H3K9 and H3K14 and Me3-H3K9 or MECP-2; Extended Data Fig. 3k,l; Extended Data Fig. 7g)[40]. Instead we found that the NCOR2 transcriptional stress checkpoint correlates with treatment resistance in patients with breast cancer in the neoadjuvant and adjuvant setting. Our studies highlight the utility of these PDOs and spheroid models as screening platforms for identifying treatment resistance

mechanisms and novel therapeutic strategies. Indeed, our results provide experimental proof of concept that gene therapy targeting of this NCOR2 transcriptional stress checkpoint could overcome resistance to C/T and immunotherapy in some solid malignancies. Certainly, application of NCOR2-targeted gene therapy using AAV- or oncolytic virus-formulated DeCOR2 or its derivatives[43] merits further investigation as a clinically viable strategy to enhance the anti-tumor efficacy of C/T, ICIs and/or other immunotherapies.

Methods

Our research complies with all relevant ethical regulations. *In vivo* experiments were performed in accordance with the guidelines from University of California, San Francisco (UCSF; CA, USA), National Health Research Institutes (NHRIs; Taiwan) and Taipei Medical University (TMU; Taipei, Taiwan). Study protocols were approved by the Institutional Animal Care and Use Committee (IACUC). Reagents and resources are listed in Supplementary Table 1.

Cell Culture and PDOs.

HMT-3522 T4–2 breast cancer cells were propagated as previously described[57]. Cells were embedded in rBM (Growth Factor Reduced Matrigel) for 12 days to generate spheroids (~100 μm)[23]. Primary breast cancer NHRI-BC-008 cells were isolated from the surgical specimen of a patient with TNBC (Tung's Metro-Harbor Hospital, Taichung, Taiwan) and propagated in IMDM (Invitrogen) supplemented with glutamine, insulin, transferrin, selenium (Lonza) and 20% FBS[59]. MDA-MB-231, T47D, HEK-293, HCC-1954, BT-474, and 4T1 cells (American Type Culture Collection) were grown on tissue culture plastic in DMEM with 10% fetal bovine serum and antibiotics. Cell lines were tested for Mycoplasma (MycoAlert Mycoplasma Detection Kit; Lonza). All cell lines were derived with authenticated sources. HCI-001 and HCI-002 PDX fragments were acquired from B. Welm (Huntsman Cancer Institute, University of Utah, UT). The PDX line BCM 2665, was acquired from M. Lewis (Baylor College of Medicine, Houston, TX)[22]. All PDOs were processed and cultivated in rBM[20,25]. All human tissues were collected using protocols approved by the Institutional Review Boards.

NCOR2 immunostaining of human breast cancer tissue.

Human breast cancer specimens were excised at Tung's Metro-Harbor (TMH) Hospital; Supplementary Table 9) from patients (n=15) pre and post neoadjuvant systemic C/T treatment (2–4 weeks). Tissues were stained using the DAKO EnVision kit (DAKO) following deparaffinization, epitope retrieval and peroxidase activity quenching. Nuclear and cytoplasmic NCOR2 staining was evaluated by a pathologist using the histological score (H-score). All human tissues were collected following informed consent using protocols approved by the Institutional Review Board (protocol number: TTMHH 104052).

RNA sequencing.

Total RNA was isolated using the RNeasy Mini Kit (QIAGEN). RNA concentration and purity were assessed by a NanoDrop Spectrophotometer. RNA integrity number (RIN) was assessed with the TapeStation. Libraries were prepared from 1 μg of RNA using

Illumina Stranded mRNA Prep (Illumina). Library concentration and quality were measured using the Qubit dsDNA HS Assay kit (Life Technologies) and Agilent High Sensitivity D1000 ScreenTape (Agilent Technologies). RNA sequencing was performed by Illumina NovaSeq 6000 platform for paired-end sequencing, 150-bp read length, for ~20 million raw reads per sample. Data analysis according to RNA sequencing FASTQ files was processed with HISAT2 Aligner in default mode with the Ensembl human transcriptome annotation (Build version GRCh38 and transcript annotation GRCh38.89). Differential gene expression analysis was performed using DESeq2 software (version 1.34.0), using an expression analysis cutoff above 1 Fragment Per Kilobase of transcript per Million mapped reads (FPKM). The fold transcript level changes (represented by FPKM) were calculated from of a list of 78 genes related to the apoptosis process (GO: 0006915) comparing paclitaxel- and vehicle-treated PDOs. The fold induction of the genes in chemo-sensitive HCI-002 *versus* chemo-resistant HCI-001 PDOs was calculated to establish the rank list (Figure 1c).

MWA analysis.

Nuclear lysates were extracted using NE-PER Nuclear and Cytoplasmic Extraction Reagents (Thermo) and immunoprecipitated with anti-IRF1 or an IgG Control antibody from independent TRAIL treated cells (1 μg/ml; 3 hours) according to the MWA protocol[30]. A repository consisting of 461 antibodies (Supplementary Table 10) to proteins linked to chromatin organization and epigenetics were assembled based on the Gene Ontology (GO) biological process terms. MWA analysis was performed at the Protein Chemistry Core Laboratory at the National Health Research Institutes (NHRIs, Chunan, Taiwan) using the Odyssey Infrared Imaging System (LI-COR Biosciences) and Odyssey software (Odyssey V3.0) to identify and quantify protein spots[30]. An “IRF1-binding index” was calculated as the ratio of the intensity of the protein spots in the anti-IRF1 immunoprecipitate to the intensity of the spots in the IgG control. Proteins with an IRF1-binding index ≥ 2 in both the anti-IRF1 co-IP experiments were considered an IRF1-binding protein with high confidence.

Induction and analysis of apoptosis.

Apoptosis was initiated by treatment with recombinant, purified human or mouse TRAIL or IFNγ (PeproTech), paclitaxel or doxorubicin or by inducing DNA damage by exposure to gamma irradiation using a Mark I Cesium 137 irradiator (JL Shepherd & Associates). Apoptosis was determined by quantifying percent active caspase 3 by indirect immunofluorescence or counting the nuclei of dead cells using the CYTOX-orange dye and normalizing dead cells to total cell number estimated by counterstaining nuclei with Hoechst 33342. In select experiments, cells constitutively expressing human nuclear histone H2B-GFP or H2B-mRFP fusion protein were used to estimate the number of cells present in the PDOs or 3D spheroids. Clonogenic survival was assessed in spheroids by measuring the size of the colonies formed by single seeded cells previously exposed to IR as a function of time (9 Gy; four weeks incubation).

Immunofluorescence and confocal imaging.

Cells were either directly fixed in 4% paraformaldehyde or ice cold 100% methanol or Triton extracted (0.1% Triton X-100 for 5 min) before fixation. Specimens were incubated with primary antibody followed by Alexa Fluor 488- or 568-conjugated secondary antibody.

Nuclei were counterstained with DAPI or Hoechst 33342. The staining of DNA double strand break repair markers, including γ-H2AX, NBS1 and KU80 was performed using a ribonuclease-based extraction protocol[60]. Cells were visualized using a Bio-Rad MRC 1024 laser scanning confocal microscope attached to a Nikon Diaphot 200 microscope. Images were recorded at 600X magnification.

Gene silencing by RNA interference.

Stable KD of *NCOR2* or *IRF1* was achieved by lentivirus-mediated RNA interference (RNAi) using validated shRNA oligonucleotides in the lentivector pLKO.1-puro (MISSION shRNA lentiviruses; Sigma-Aldrich; Supplementary Table 1). Stable KD of *TP53* expression was achieved by lentivirus-mediated RNAi using validated shRNA sequences (RFP-hp53 fusion, GeneTarget, San Diego, CA; pRFP-CB-shLenti shRNA, Origene, Rockville, MD). KD of *HDAC3* expression was achieved by retroviral-mediated RNAi using published oligonucleotide sequences[61]. Infection was verified by quantitative real-time PCR (qRT-PCR) and immunoblot (IB) analysis. Lentivirus-mediated genetic KD of breast cancer PDO cells was as described[62].

Overexpression vectors.

Retroviral inducible expression of EGFP-epitope tagged NCOR2 was prepared by subcloning murine *NCOR2* cDNA (e isoform) from pCMX-FLAG-NCOR2 (M. A. Lazar, University of Pennsylvania)[63] into pBluescriptII KS+ (Stratagene). N-terminal HA-epitope tag was added by re cloning into a modified hybrid Epstein-Barr virus/retroviral vector pLZRS-MFG-*tet*-EGFP with a tetracycline (tet) regulated promoter[64,65] yielding the pLZRS-MFG-*tet*-HA-EGFP-NCOR2 construct. Mutant NCOR2 (K449A) was constructed using the QuickChange Site-Directed Mutagenesis kit (Stratagene) and pMFG-*tet*-HA-EGFP-NCOR2 as template. To construct a tet-regulated expression system for IRF1, IRF1 cDNA was removed from pcDNA3-IRF1 (J. Park, Sungkyunkwan University, Seoul, Korea)[66] using BamHI and XhoI and cloned between BamHI and XhoI sites of the multiple cloning site of the lentiviral vector pLV-puro-Tet-MCS-IRES-EGFP. The Ran GTPase mutant Ran (Q69L) (Jia-Lin Lee, National Tsing Hua University, Taiwan)[67] was PCR-amplified and subcloned into the lentiviral expression vector pLVX-IRES-Puro. Amphotropic retrovirus was produced in modified 293 cells or in Phoenix ampho cells (G. Nolan, Stanford University) with packaging vectors pCgp and pVSVG to boost viral titer. Cells were spin infected with retrovirus carrying wild-type or mutant NCOR2, followed by infection with a high titer MFG virus expressing the tetracycline-controlled transcriptional transactivator produced in the packaging cell line 293GPG[68]. Cells expressing wild type or mutant NCOR2 or mutant NCOR2 were expanded in the presence of tet (1 μg/mL) and wild type or mutant NCOR2 expression was induced by withdrawal of tet (2–4 days), followed by FACS sorting for GFP positive cells and expansion in the presence of tet. Level of gene expression and/or knockdown was verified by qRT-PCR and confirmed through immunoblot analysis. Expression of the mutant Ran (Q69L) was detected using the TaqMan® Assay (ThermoFisher Scientific).

Construction of DeCOR2.

The truncated human NCOR2 protein, "Decoy of NCOR2 (DeCOR2)", which spans from amino acids 395–700 of the full length human NCOR2, consists of the previously identified deacetylase activating domain (DAD; amino acids 395–489)[69], a high confidence nuclear localization signal (NLS; amino acids 680–685; predicted by *in silico* tools, including cNLS mapper, NLStradamus, NoD, Nuclear Protein Database, NucPred, and SeqNLS), and the intervening sequence. Primers 5'-CTTTGGAACTGAATTCGCCACCATGATCCCGCCCATGCTG-3' and 5'-TGAGGCCTAGCGGCCGCTCACGTAGAATCGAGACCGAGG-3' were synthesized and used to amplify the DeCoR2 from a full-length human NCOR2 expression construct. The DNA encoding the murine version of DeCoR2 (mDeCoR2), which corresponds to amino acids 395–696 of the full-length murine NCOR2 (isoform 1), was synthesized by the PRIME Gene Synthesis and Subcloning service of GeneDireX, *Inc.* (Taiwan). The amplicon of human DeCOR2 or the synthesized mDeCOR2 DNA was subcloned into a V5 epitope- and polyhistidine-tagged expression vector pcDNA3.1/V5-His B using the In-Fusion® HD Cloning Kit to generate the plasmid pcDNA3.1-V5-His B-DeCOR2. The sequence of the construct was verified using a forward T7 promoter primer and a reverse BGH primer. For stable gene expression the DeCOR2 expression cassette was subcloned into the retroviral vector pMXs-IRES-Blasticidin or the lentiviral vector pLVX-IRES-Puro using the In-Fusion® HD Cloning Kit. For the construction of DeCOR2 (3×LT NLS), the intrinsic NLS sequence corresponding to full-length NCOR2 a.a. 680 to 685 (RRKKKK) was replaced by triplicated NLS derived from SV40 large T (LT) antigen present on the pShooter™ vector (pCMV/myc/nuc; Invitrogen). The whole construct was synthesized and then digested by EcoRI and HindIII and cloned into a pAAV-MCS expression vector. For the construction of the tet-regulated expression vector of mDeCOR2, the DNA sequence of mDeCOR2 was cloned into a PiggBac transposon system vector engineered with a Myc-tag and IRES GFP. Cells were stably transduced with reverse tet-controlled transactivator (rtTA, tet-on system) lentivirus (pLV-neo). After neomycin (100 μg/mL) selection of rtTA-integration, cells were co-transfected (Lipofectamine 3000, Thermo Fisher, per manufacturer's recommendation) with the PiggyBac vector expressing mDeCOR2 and PiggyBac transposase. Cells were selected for mDeCOR2 and GFP expression by FACS.

Mice.

Female Nude, NOD/SCID, BALB/c, and *RAG1*$^{-/-}$ (C.129S7(B6)-Rag1^{tm1Mom}/J) and NSG™ mice (Jackson Laboratory) were housed four per cage and maintained in a pathogen-free, barrier-protected environment at UCSF, NHRIs, or TMU animal facility (Taipei, Taiwan).

Xenograft breast tumorigenesis models and treatment.

Cancer cells were lentivirally transduced with an EGFP and firefly luciferase (FF-Luc) fusion vector and the GFP-positive cells were sorted by FACS. Cells (2×10^6 cells in 100 μl 1:1 mixture of Matrigel and HBSS) were inoculated orthotopically into the mammary fat pads of 8-week-old female NOD/SCID mice or BALB/c mice (for syngeneic models) or subcutaneously into the flanks of 8-week-old female nude mice. Ten days post inoculation,

when tumor bulk was similar between the two groups (similar bioluminescence imaging [BLI] intensity and palpable tumor size), mice were given intraperitoneal (IP) injections of paclitaxel (20 mg/kg) or doxorubicin (7.5 mg/kg) or vehicle every week for 4 consecutive weeks. In selected syngeneic tumor models, the mice received IP injections of the anti-PD1 antibody (10 mg/kg; Bio X Cell) or a control IgG twice weekly for 4 consecutive weeks. Tumor mass was assessed by BLI weekly before each treatment. Relative tumor bulk was determined by calculating the ratio of the BLI signal intensity of the tumor at a given time and that of the initial tumor size (*i.e.* at time of treatment initiation). For PDX studies human breast tumor fragments derived from a triple-negative ($ER^-PR^-HER2^-$) (TM00999) were injected orthotopically into NSG™ mice (Jackson Laboratory). Mice were administered with weekly paclitaxel or vehicle intraperitoneally with or without intra-tumoral (IT) injections of AAV-DJ-DeCOR2 or control virus once tumors became palpable; see below. The tumors were calipered weekly to monitor growth kinetics. Tumor volumes were calculated using the formula $1/2 \times \text{length} \times (\text{width})^2$. The animals were euthanized 31 days following initiation of treatment or when the maximum tumor diameter approved by the IACUC was exceeded. In the syngeneic breast tumor model, 4T1 mouse breast cancer cells were inoculated into the mammary fat pads or subcutaneously into the flanks of 8-week-old female BALB/c mice. The tumors were removed for IHC or flow cytometry analyses 2–4 weeks following initiation of treatment. The maximal tumor size permitted by the IACUCs is 20 mm in diameter or 4,000 mg in weight, a limit that was not exceeded in our experiments.

In vivo gene transfer and gene therapy.

DeCOR2 gene therapy was performed using a recombinant AAV-mediated *in vivo* gene transfer system. Briefly, the cDNA encoding C-terminal V5-epitope-tagged DeCOR2 present in the plasmid pcDNA3.1-V5-His B-DeCOR2 was subcloned into a recombinant AAV vector pAAV-MCS and pAAV-IRES-GFP[44] using the In-Fusion® HD Cloning Kit to generate the plasmids pAAV-V5-DeCOR2 and pAAV-V5-DeCOR2-IRES-GFP, respectively. The DNA encoding mDeCoR2 with a tail V5-tag, and the pUC57-amp vector was synthesized, digested by ECoRI and Hind III and then subcloned into the pAAV-MCS vector. To generate the virus, 293AAV cells, which stably express the adenovirus E1 gene, were co-transfected with pAAV-RC, pHelper and pAAV-V5-DeCOR2 or pAAV-V5-DeCOR2-IRES-GFP and the cells were harvested and subjected to several rounds of freeze/thaw cycles followed by high-speed centrifugation (10,000 × *g*) to collect the crude AAV supernatant, which was then purified using a ViraBind AAV purification Kit. The titer of the purified viral particles, designated AAV-DJ-V5-DeCOR2, was quantified by genome copy (GC) number using the QuickTiter AAV Quantitation Kit. The virus encoding mDeCOR2, AAV-DJ-V5-mDeCOR2, was cloned and generated similarly. Breast cancer cells were inoculated into the mammary fat pads of NOD/SCID mice, and after two weeks, when the size of the tumors reached approximately 100 mm^3, the animals received IT injections of the AAV-DJ-V5-DeCOR2 virus or the control AAV-DJ virus (1×10^{12} GC per tumor). Mice were injected every 3 days for a total of 5 doses to achieve persistent expression of V5-epitope-tagged DeCOR2 in the tumor cells (Fig. 6h). Four days following the first dose of gene therapy, the mice were given IP injections of paclitaxel (20 mg/kg) or vehicle every week for 4 consecutive weeks and tumor bulk was monitored using BLI. The virus was

injected into the PDX tumor 3–4 weeks post-engraftment when tumors became palpable using an identical protocol. In the 4T1 syngeneic mouse tumor model, the mice received IP injections of anti-PD1 antibody (twice weekly for 4 consecutive weeks) 4 days following the first dose of gene therapy.

BLI.

BLI was performed using the IVIS Imaging System (Xenogen; NHRIs and TMU, Taiwan) or within the IACUC animal barrier at UCSF (San Francisco, USA). Mice were anesthetized with 2% isoflurane and injected intraperitoneally with 150 mg/kg D-luciferin 6 min before image acquisition. Tumor bulk was determined by measuring the photon flux from a region of interest drawn around the bioluminescence signal using Live Imaging Software (Xenogen/PerkinElmer). At experiment termination mice were sacrificed, lesions were dissected, measured, and macroscopically analyzed, fixed in 4% paraformaldehyde, paraffin embedded, and H&E sections were evaluated for histopathological analysis.

qRT-PCR.

Total RNA was extracted and purified using the RNeasy Mini Kit (Qiagen) and total RNA (1.0 μg) was used as a template for cDNA synthesis using MMLV reverse transcriptase (Promega). cDNA (100 ng) was used as template for PCR amplification using the LightCycler FastStart DNA MASTER^{PLUS} SYBR Green I Kit and the LightCycler System (Roche). Oligonucleotide primers were designed using LightCycler Probe Design Software 2.0 (Roche) or Primer Bank (http://pga.mgh.harvard.edu/primerbank/index.html) (Supplementary Table 1). Transcript expression was quantified by normalizing the gene of interest copy number (per μL) to absolute levels of an endogenous, stably expressed reference gene, ribosomal protein L13a (*RPL13A*).

Nuclear fractionation and IB analysis.

Trypsinized cells were centrifuged (100 × *g*), and cell pellets were washed with PBS and lysed by suspension (10 min, 4°C) in Buffer A (10mM HEPES, 1.5mM $MgCl_2$, 10mM KCl, and 0.05% NP-40 [pH7.9]) in the presence of protease and phosphatase inhibitors. Lysates were centrifuged (10 min, 4°C, 14,000 × *g*). Supernatants (cytoplasmic fractions) were dispensed, and the pellets were washed with Nuclear Wash Buffer (10mM HEPES, 1.5mM $MgCl_2$, 10mM KCl [pH7.9]) (6x) and the pellets were incubated with ice-cold Buffer B (5mM HEPES, 1.5mM $MgCl_2$, 0.2mM EDTA, 26% glycerol (v/v), 300mM NaCl [pH7.9]) all in the presence of protease and phosphatase inhibitors. The pellets were, sonicated and the nuclear lysates were incubated (30 min, 4°C) and re-centrifuged (20 min, 4°C, 16,100 × *g*) and the final nuclear supernatant was collected and subjected to IB analysis.

HDAC activity assay.

HEK 293 cells were infected with retroviral constructs expressing an inducible myc tagged NCOR2, NCOR2 (K449A) or a control EGFP (pLZRS-MFG-*tet*-myc(4)-EGFP-NCOR2, pLZRS-MFG-*tet*-myc(4)-EGFP-NCOR2 (K449A) or pLZRS-MFG-*tet*-myc(4)-EGFP). Myc tagged protein expression was induced through doxycycline treatment (1 μg/mL; 16 hours) and nuclear protein extracts were prepared[70]. Briefly, cells were scraped and collected in

PBS, swollen in a hypotonic buffer (10 mM HEPES pH 7.9, 1.5 mM $MgCl_2$, 10 mM KCl, 1 mM EGTA, 0.5 mM DTT, 0.2 mM PMSF, 0.1% NP40) and homogenized (4°C). Nuclei were separated via centrifugation (2,000 × *g*) and treated with high salt buffer (20 mM HEPES, 1.5 mM $MgCl_2$, 1.2 M KCl, 0.2 mM EDTA, 1 mM EGTA, 0.5 mM DTT, 0.2 mM PMSF, 0.1% NP40) and nuclear extract (600 μg) was pre incubated with protein G agarose beads (50 μL; Invitrogen) equilibrated in diluent buffer (15 mM HEPES pH 7.9, 1 mM $MgCl_2$, 0.2 mM EDTA, 150 mM KCl, 20% glycerol, 0.5 mM DTT, 0.2 mM PMSF; 1 hour, 4°C). Nuclear lysate was transferred and incubated (4°C; 3 hours) with 50 μL of equilibrated protein G agarose beads (Invitrogen) and mouse anti-myc antibody (5 μg). Beads were washed (3X) with wash buffer (diluent buffer with 0.5 M KCl) and once with diluent. Washed conjugated beads were used in the Fluor de Lys Assay System per kit instructions to determine HDAC activity associated with the immunoprecipitation. Fluorescence was determined using a Spectra Max M5 flourimetric plate reader (Molecular Devices).

ChIP.

ChIP experiments (triplicates) used primers specific for IRF1 consensus binding sites, IRF-E, in the promoter regions of TRAIL (*TNFSF10*), STAT1 (*STAT1*), caspase 1 (*CASP1*), caspase 7 (*CASP7*), and NFκB p65 (*RELA*), as reported and indicated in sequence databases from TRANSFAC (http://www.gene-regulation.com/pub/databases.html) and SABiosciences (EpiTect ChIP qPCR Primers, Qiagen)[28,71]. Briefly, samples were immunoprecipitated (5 μg/ml) with specific or nonspecific antibody. ChIP-enriched chromatin (2–5 μl) was subjected to ChIP-PCR and enriched regions were assessed relative to control IgG or reference cells. Re-ChIP experiments were performed by using the Re-ChIP-IT Magnetic Chromatin RE-Immunoprecipitation kit according to the manufacturer's protocol (Active Motif, Carlsbad, CA, USA).

Immunofluorescent staining and confocal imaging.

Immunofluorescent staining of cell monolayers, spheroids and PDOs was as described[72]. Confocal imaging was performed using a Nikon Digital Eclipse C1 confocal microscope system.

Reporter assays.

Cells were transduced with the IRF1 or IFNγ luciferase reporter lentivirus (Cignal Lenti Reporter; Qiagen) and reporter activity was measured by using the ONE-Glo™ Luciferase Assay System (Promega, Madison, WI).

Flow cytometry analysis.

Cells were dissociated, antibody-labeled (1–2 μg per 10^6 cells × 1 hr) and resuspended in HBSS/2% FBS. Flow cytometry was done using a FACSCanto™ II flow cytometer (BD Biosciences) with appropriate gating (Supplementary Fig. 1). Cell sorting was performed using a FACSAria™ III cell sorter (BD Biosciences). All data were analyzed with FlowJo software (Tree Star, Inc., Ashland, OR, USA, version 10.5.3)

Microarray experiments.

Total RNA (triplicates; 3 independent preparations) was prepared using TRIzol™ and purified using a RNeasy Mini Kit with DNase treatment (Qiagen). To prevent apoptosis, cultures were pretreated with caspase inhibitors DEVD-CHO and Ac-IETD-CHO (1 μM) added prior to TRAIL treatment. Gene expression analysis was performed on an Affymetrix GeneChip™ Human Genome U133A 2.0 platform containing 22,283 probes. Biotinylated cRNA was produced from total RNA. Following hybridization, washing and staining, arrays were scanned using a confocal scanner. The hybridization intensity data was processed using the GeneChip Operating software. Affymetrix .cel files (probe intensity files) were processed with ArrayAssist Lite (v3.4, Stratagene). Files were imported and processed with the GC-RMA algorithm to yield probe set intensities and additionally, Affymetrix Preset, Absent, Marginal flags were computed. Values were exported in .chp files, which were thereafter imported into the Partek Genomics Suite software (v6.2). A filtering criterion ($P < 0.01$ by Student's t test, fold-change > 2.0-fold) was used to select differentially expressed genes within a comparison group. To select genes that were differentially induced or repressed in response to NCOR2 and TRAIL treatment, the GC-RMA expression values of all the 16 transcriptomes were log2 transformed and a two-way ANOVA was calculated, yielding 3 *P* values for each gene. Controls included genes whose modulation reflects whether the gene's expression is significantly different before and after NCOR2 expression, with and without TRAIL treatment, and whether differential expression of the gene in response to TRAIL depends upon the presence or absence of NCOR2. Additional pair wise contrasts were performed for each of the 4 paired conditions, yielding both *P* values and fold changes between the mean expression values of the different conditions. The difference between TRAIL-induced changes in the level of gene expression between T4–2-NCOR2 cells and T4–2-vector cells was measured by using the equation "$\log_2$ (NT/N) - $\log_2$ (VT/V)", which was designated as a *differential response index* (*DRI*). A filtering criterion ($P < 0.05$ by two-way ANOVA, $DRI \geq 1.0$ or ≤ -1.0) was used to select genes that were differentially responsive to TRAIL between T4–2-NCOR2 and the T4–2 vector control cells.

Bioinformatics analysis.

Hierarchical clustering of the selected genes was performed using Cluster and TreeView software. The enriched transcriptional factor binding motifs in the promoter regions of genes in the NCOR2-associated gene sets were searched using the oPOSSUM program (http://www.cisreg.ca/cgi-bin/oPOSSUM/opossum). Over-represented transcriptional factor binding motifs were determined by Z-score and the one-tailed Fisher exact probability test[73]. A Z-score of 10 or greater and/or a Fisher probability value of 0.05 or smaller was deemed statistically significant. The IRF1 and the STAT1 transcriptional factor binding motifs were further curated by a transcriptional factor binding site database DECODE (http://www.sabiosciences.com/chipqpcrsearch.php?app=TFBS&qs=1304904552; Qiagen).

Data mining of the gene expression profiles of tumors and clinical cancer specimens.

The transcript levels of *NCOR2* in the pretreated tumor specimen from 111 breast cancer patients who had received pre-operative combination chemotherapy with adriamycin-cyclophosphamide (AC) or AC versus paclitaxel (AC + T) and the associated clinical and

pathological information were downloaded from the Breast Cancer I-SPY 1 Trial database (I-SPY 1 data; February 2011)[34]. The transcript levels of *NCOR2* in the pretreated tumor tissues of 24 breast cancer patients who were neoadjuvant treated with docetaxel were downloaded from NCBI's Gene Expression Omnibus (accession number GSE6434)[35]. Gene expression profiles of the pretreated breast cancer tissues from the 82 breast cancer patients who were neoadjuvant treated with epirubicin and cyclophosphamide (the EC regimen) were provided by Siemens Healthcare Diagnostics Products GmbH[36]. The Affymetrix probe set *207760_s_at* that displayed the highest hybridization intensity for *NCOR2* was used for the analysis. Patients with pathologically defined complete absence of invasive carcinoma in the breast following neoadjuvant chemotherapy were classified as "responders" and those who displayed only partial response, or no response were classified as "nonresponders" of neoadjuvant chemotherapy.

Statistics and reproducibility.

Sample size, indicated in figure legends, was not pre-determined. Sample size was dictated by estimation of statistical robustness based upon prior published studies[74]. Data distribution was assumed to be normal, but not formally tested. In some *in vivo* studies, tumor growth was quite rapid and the animals were sacrificed prior to study termination for ethical reasons, necessitating their exclusion from analysis. Poor quality data were excluded from flow cytometry data following evaluation by FlowJo software. PDO studies were randomized whereas all other *in vitro* experiments were not. Allocation of mice into experimental treatment groups was based on the average BLI or tumor volume ensuring all groups had no significant differences in tumor size at the start of the study. However, investigators were not blinded to allocation during experiments and outcome assessment. Experimental robustness was assured by inclusion of multiple investigators, including those not involved in the experimental manipulation in data analysis. Information regarding experimental replicates are included in the figure legends. All tests were two-sided and not adjusted for multiple comparisons. Differences between groups were considered statistically significant at values of $P \leq 0.05$. The exact P values associated with the figure panels are listed in Supplementary Table 11. A cutoff value that best discriminates between groups with high or low *NCOR2* expression with respect to treatment response was determined using the maximal Youden's index[75]. All reported data represent biological replicates. Survival curves were generated using the Kaplan-Meier method. The curves were plotted and compared using the unpaired log-rank test using the GraphPad Prism 6.01 software (GraphPad Software, La Jolla, CA, USA). Raw numerical data and statistical analysis of all repeats for all figures and extended data are provided in Source Data.

Reporting Summary.

Further information on research design is available in the Nature Research Reporting Summary linked to this article.

Data availability.

All data used to generate results is located in Extended Data and Supplementary Information. The RNA sequencing data reported in Fig. 1 are available at the Gene Expression Omnibus (GEO) under accession code GSE183477. The raw and analyzed

data from the microarray experiments are available at the GEO under accession codes GSE138900 and GSE8346. Re-analyzed, previously published gene expression data are available under accession code GSE6434 or can be requested from the authors including I-SPY 1 Trial Investigators or Siemens Healthcare Diagnostics Products GmbH. Source data have been provided as Source Data files. All other data supporting the findings of this study are available from the corresponding author on reasonable request.

Methods-only References

Extended Data

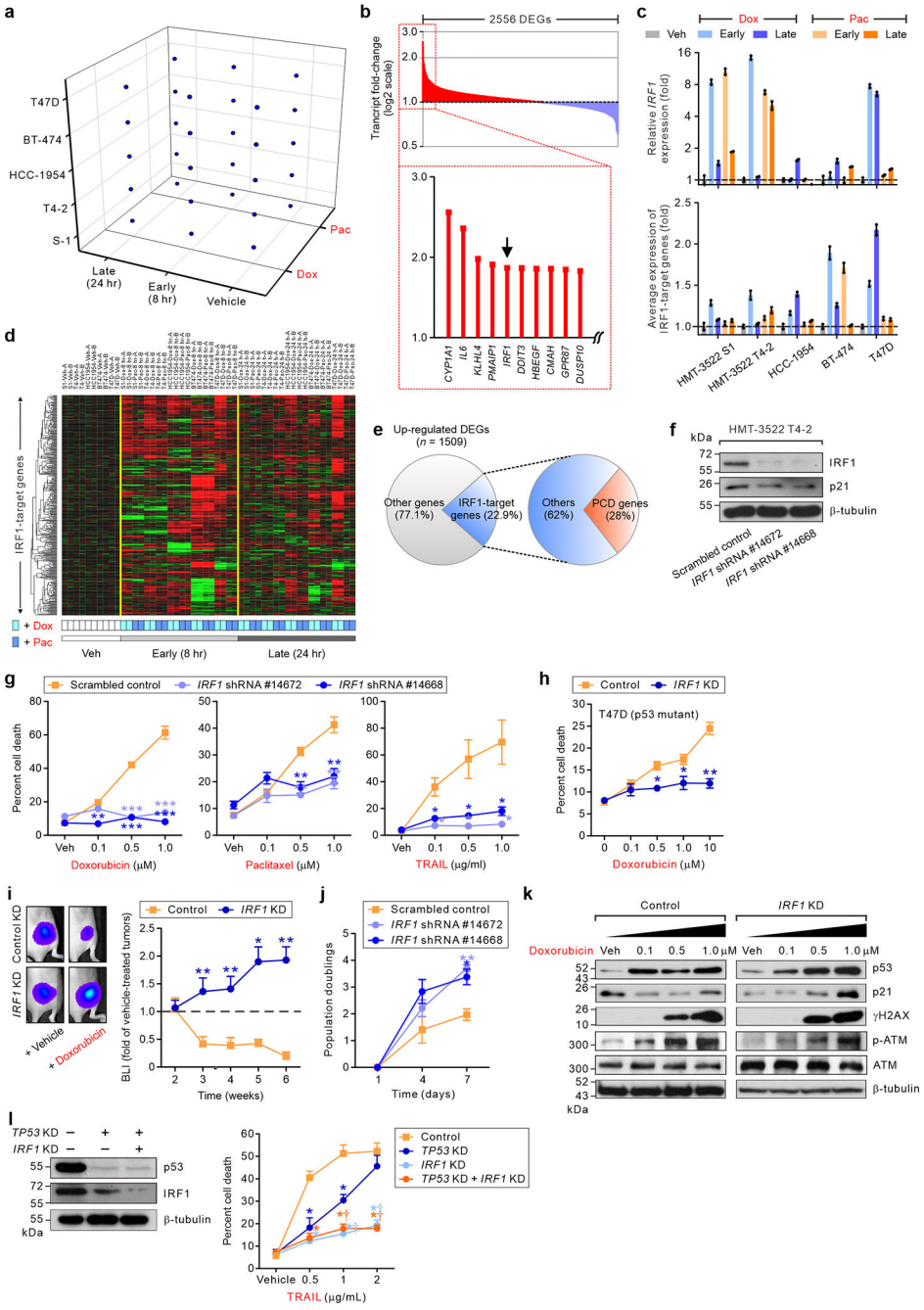

Extended Data Fig. 1. IRF1 and its role in cytotoxic stress-induced cell death

a, Pre-malignant (HMT3522 S-1) mammary epithelial cells, and breast cancer cell lines including: HMT3522 T4–2, HCC-1954, BT-474 and T47D cells were treated with vehicle (Veh), doxorubicin (Dox; 1 μM) or paclitaxel (Pac; 500 nM) and their gene expression was profiled at early (8 hr) or late (24 hr) time points following treatment initiation. The blue dots represent each of 30 combinations of the different cell lines studied,

the chemotherapeutic agents used, and the treatment time points examined. **b**, *IRF1* as the conserved, top ranked, transcription factor induced by chemotherapeutic agents in **a**. **c**, The transcript level of *IRF1* (top) and the average transcript level of putative IRF1-target genes (bottom), in Veh-, Dox- or Pac-treated breast cancer cell lines (n=2 independent experiments). **d**, Hierarchical clustering of putative IRF1-target genes that exhibited differential expression between the Veh- and Dox- or Pac-treated breast tumor cell lines. **e**, The IRF1-target genes up-regulated in chemotherapeutic agent-treated breast tumor cells in **d**. **f**, Knockdown (KD) of *IRF1* expression in HMT-3522 T4–2 breast cancer cells using two different shRNAs (representative data of n=2 independent experiments with similar results). **g**, The percent cell death in HMT-3522 T4–2 cells expressing a scrambled shRNA or an *IRF1* shRNA treated with doxorubicin, paclitaxel, or TRAIL (n=3 independent experiments). **h**, The percent cell death of P53-mutant T47D breast cancer cells with shRNA-mediated knockdown (KD) of *IRF1* or a scrambled shRNA (control) treated with doxorubicin (n=3–5 independent experiments, the exact n are provided in the numerical source data). **i**, Bioluminescence imaging (BLI) of flank regions of nude mice inoculated with scrambled control- or *IRF1*-shRNA (*IRF1* KD) expressing HCC-1954 cells four weeks following systemic treatment with doxorubicin (n=2–5 mice per group, the exact n are provided in the numerical source data). **j**, The rate of growth of scrambled shRNA- and *IRF1*-shRNA-infected HMT-3522 T4–2 cells (n=3 independent experiments). **k**, Representative immunoblots of p53, p21, γH2AX, and total and phospho-ATM (S1981; p-ATM) in HMT-3522 T4–2 cells with KD of *IRF1* expression or a scrambled shRNA (control) treated with doxorubicin (24 hr). **l**, IRF1 contributes to cytotoxic stress-induced cell death independent of p53 status (n=4 independent experiments). Data are presented as mean ± s.e.m. (**c,g–j,l**). *P < 0.05; **P < 0.01; ***P < 0.001 *versus* control (**g,h,i,j**); *P < 0.05 *versus* control; †P < 0.05 *versus P53* KD (**l**), two-tailed unpaired Student's t-test.

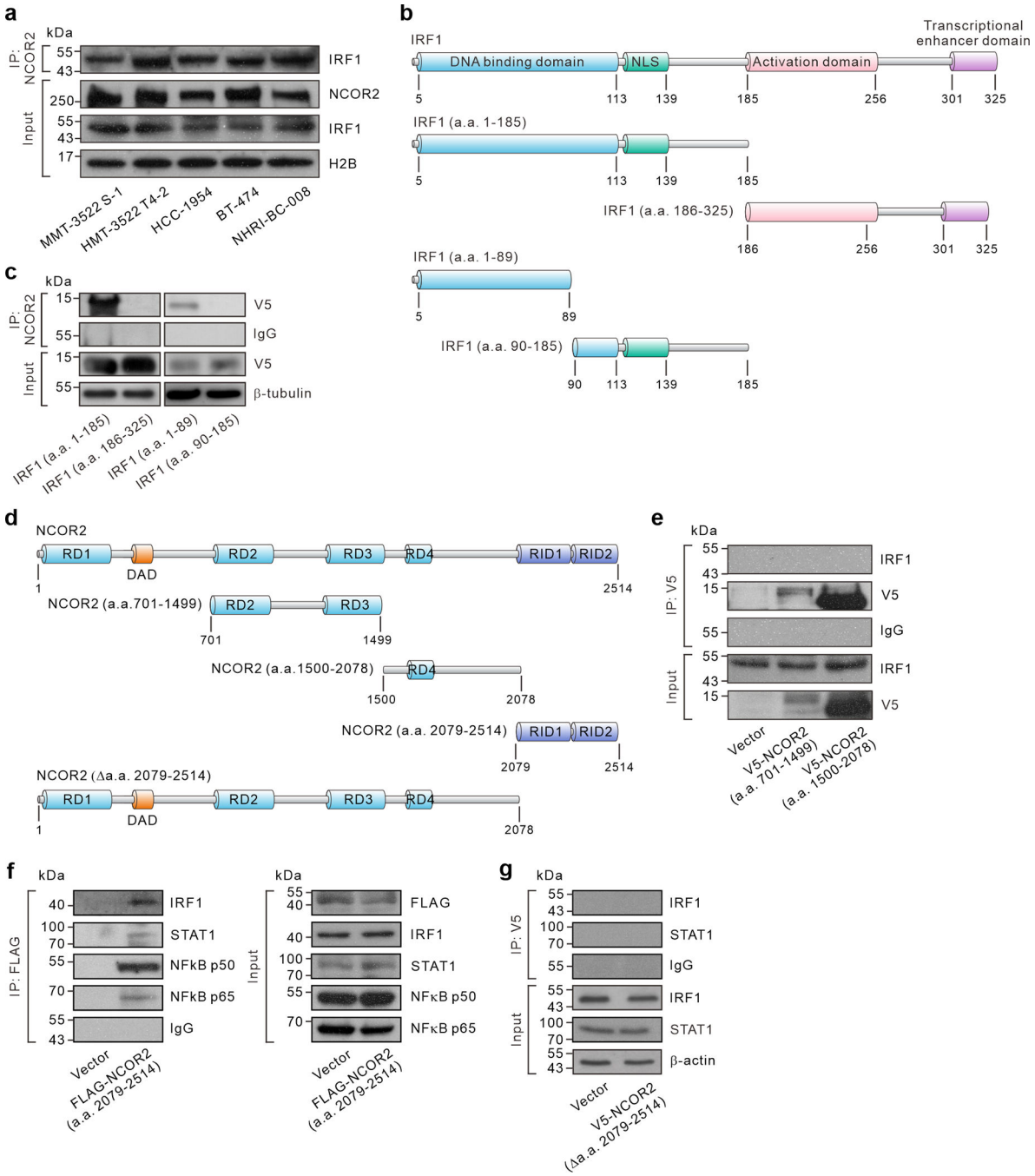

Extended Data Fig. 2. The protein domains mediating the IRF1–NCOR2 interaction

a, Co-immunoprecipitation (IP) of *IRF1* with NCOR2 in the nuclear lysates of HMT-3522 S-1 mammary epithelial cells, HMT-3522 T4–2 neoplastic mammary epithelial cells, HCC-1954, BT-474 breast tumor cell lines and in primary patient breast cancer NHRI-BC-008 cells. Cells were pre-treated with TRAIL (1 μg/ml) and the cell lysates were collected at 3 hours post-treatment. Histone 2B (H2B) was included as a loading control (representative data of n=2 independent experiments with similar results). **b**, The functional domains of *IRF1* and the various truncated mutants. NLS, nuclear localization signal;

a.a., amino acid. **c**, The N-terminal region (a.a. 1–185) as the NCOR2-binding region (NBD) of *IRF1*. MDA-MB-436 breast cancer cells were transfected with the V5-epitope-tagged truncated *IRF1* mutants depicted in **b** and the nuclear lysate was subjected to co-IP (representative data of n=2 independent experiments with similar results). **d**, The functional domains of NCOR2, its fragments and a C-terminal truncated NCOR2 protein (NCOR2 Δa.a. 2079–2514). RD, repressor domain; DAD, deacetylase-activating domain; NLS, nuclear localization signal. RID, nuclear receptor interaction domain. **e**, The NCOR2 protein fragments NCOR2 (a.a. 701–1499) and NCOR2 (a.a. 1500–2078) do not interact with endogenous IRF1. MDA-MB-436 cells were transfected with V5-epitope-tagged NCOR2 protein fragments and the nuclear lysate was subjected to co-IP using anti-V5 antibody or an isotype matched IgG. Shown are representative IB of IRF1 and V5 in the immunoprecipitated lysate, and in the total cellular lysate (input) (representative data of n=2 independent experiments with similar results). **f**, The C-terminal region of NCOR2 (NCOR2 a.a. 2079–2514) interacts with IRF1, STAT-1, and NF-κB p50 in MDA-MB-436 cells. Shown are IB of IRF1, NF-κB p50, NF-κB p65 and STAT-1 in the immunoprecipitated lysate (representative data of n=2 independent experiments with similar results). **g**, The C-terminal truncated NCOR2 (NCOR2 Δa.a. 2079–2514) fails to interact with *IRF1* and STAT-1 in MDA-MB-436 cells. Shown are IB of *IRF1* and STAT-1 in the immunoprecipitated lysate (representative data of n=2 independent experiments with similar results).

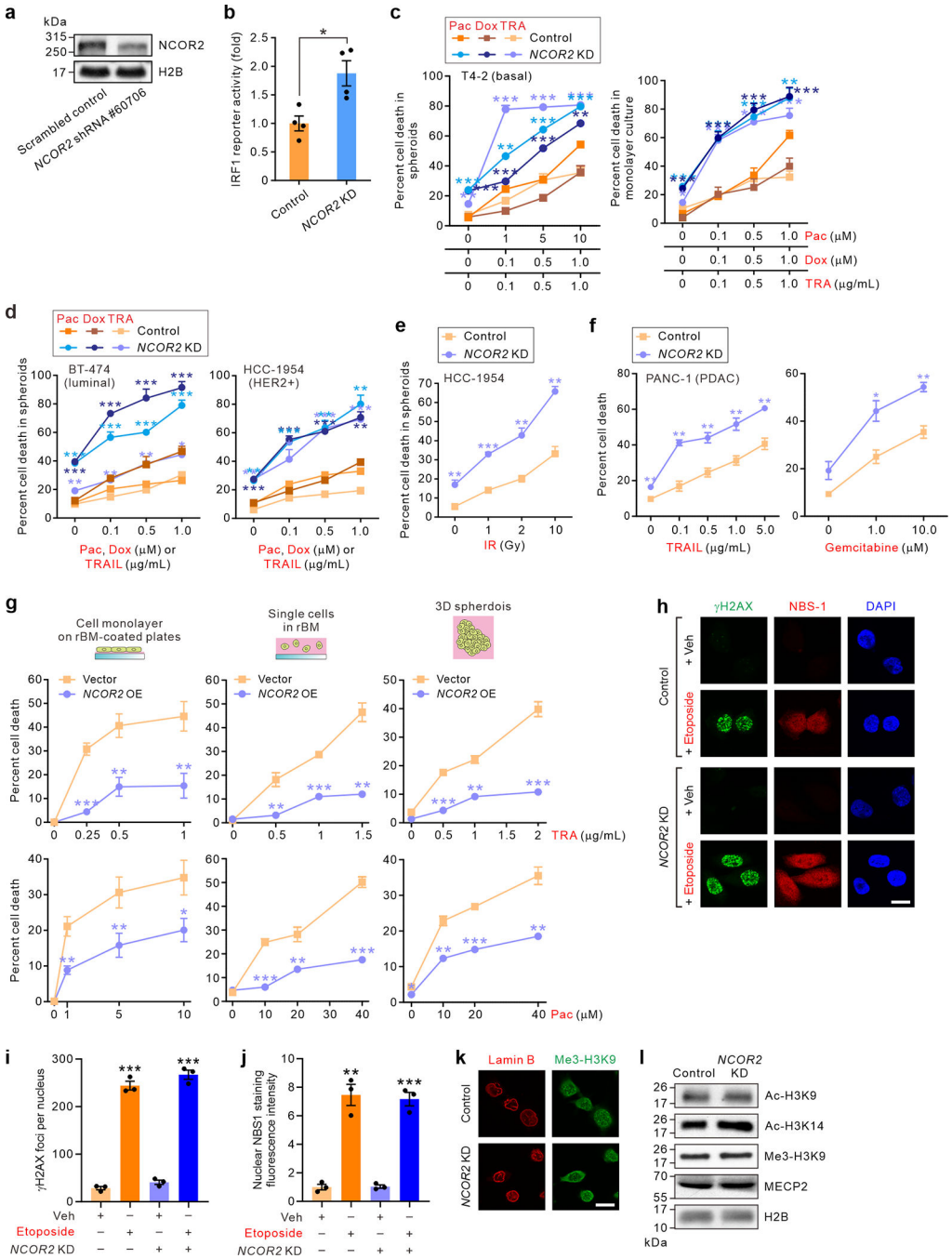

Extended Data Fig. 3. Knockdown of *NCOR2* sensitizes breast cancer cells to cytotoxic stress

a, Knockdown (KD) of *NCOR2* expression in HMT-3522 T4–2 breast cancer cells using a shRNA vector (clone #60706) (representative data of n=2 independent experiments with similar results). **b**, The transcriptional activity of IRF1 in HMT-3522 T4–2 cells with KD of *NCOR2* expression (n=4 independent experiments). **c**, KD of *NCOR2* expression rendered HMT-3522 T4–2 cells hypersensitive to paclitaxel (Pac), doxorubicin (Dox), or TRAIL (TRA)-induced apoptosis (n=3 independent experiments). **d**, KD of *NCOR2* expression rendered BT-474 or HCC-1954 spheroids hypersensitive to cytotoxic stress-induced death

(*n*=3 independent experiments). **e**, HCC-1954 spheroids with KD of *NCOR2* expression are more sensitive to ionizing radiation (IR)-induced cell death (*n*=3–4 independent experiments, the exact n are provided in the numerical source data). **f**, KD of *NCOR2* expression rendered pancreatic ductal adenocarcinoma (PDAC) PANC-1 cells hypersensitive to TRAIL- or gemcitabine-induced death (*n*=3 independent experiments). **g**, The percent cell death of vector- or *NCOR2*-overexpressed (OE) HMT-3522 T4–2 cells grown as a 2D cell monolayer on rBM-coated plates (left) or as single cells (middle) or three-dimensional (3D) organoids embedded within rBM (right) following exposure to increasing doses of TRA or Pac (*n*=3 independent experiments). **h**, Immunofluorescence staining of γH2AX and NBS1 in vehicle (Veh)- or Etoposide (1 μM × 24 hr)-treated HMT-3522 T4–2 cells with lentiviral-shRNA-mediated KD of NCOR2 expression or infected with a scrambled shRNA. Scale bar, 20 μm. **i**,**j**, The number of γH2AX nuclear foci (**i**) and the fluorescence intensity of nuclear NBS-1 staining per cell (**j**) in cells described and treated in **h** (*n*=3 independent experiments). **k**, Immunofluorescence images in HMT-3522 T4–2 cells with shRNA-mediated KD of *NCOR2* expression or infected with a scrambled shRNA stained with lamin B and a marker of histone trimethylation H3K9 (Me3-H3K9). Scale bar, 20 μm. **l**, Total nuclear acetylated (Ac) histone H3K9 (Ac-H3K9), Ac-H3K14, Me3-H3K9 and methyl-CpG binding protein 2 (MECP2) in HMT-3522 T4–2 cells with shRNA-mediated KD of NCOR2 expression or infected with a scrambled shRNA (representative data of *n*=2 independent experiments with similar results). Data are presented as mean ± s.e.m. (**b,c–g,i,j**). **P* < 0.05; ***P* < 0.01; ****P* < 0.001 *versus* control (**b–f**), vector (**g**) or vehicle (**i,j**), two-tailed unpaired Student's *t*-test.

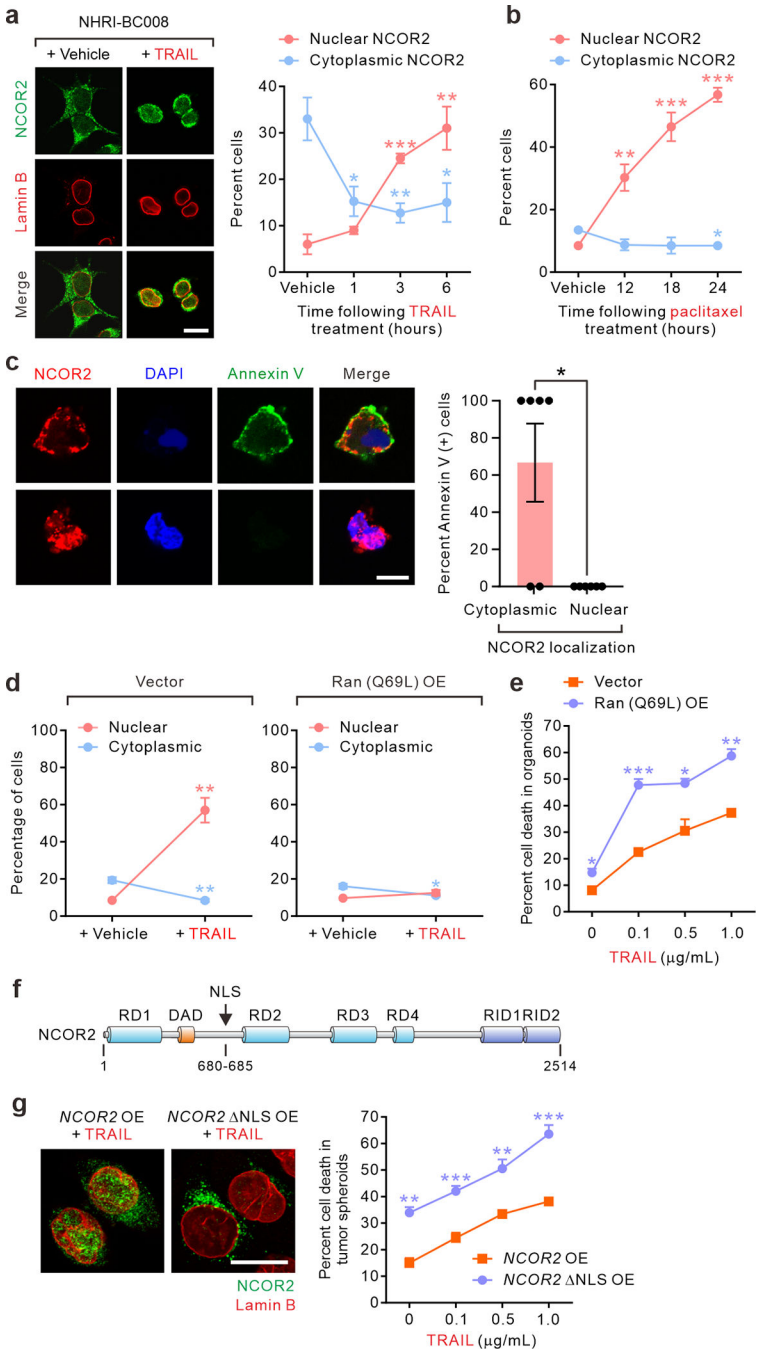

Extended Data Fig. 4. Cytotoxic stress-induced nuclear translocation of NCOR2

a, Left: Immunofluorescence staining of NCOR2 in vehicle- or TRAIL-treated primary breast cancer NHRI-BC-008 cells. Right: The percentage of cells displaying nuclear *versus* cytoplasmic localized NCOR2 following exposure to TRAIL (n=4 independent experiments). Scale bar, 20 μm. **b**, The percentage of NHRI-BC-008 cells displaying nuclear *versus* cytoplasmic localized NCOR2 following exposure to paclitaxel (1 μM) (n=4 independent experiments). **c**, Immunofluorescence staining of NCOR2, DAPI (cell nuclei), and the early apoptosis marker Annexin V in NHRI-BC-008 cells 1 hour following

treatment with TRAIL (1 μg/ml). Scale, 10 μm. Right: The percentage of cells with positive Annexin V staining in cells with mainly nuclear *versus* those with mainly cytoplasmic localized NCOR2 (n=100 cells counted per experiment, n=6 independent experiments). **d**, The TRAIL-induced nuclear *versus* cytoplasmic localization of NCOR2 in HMT-3522 T4–2 cells infected with and without the mutant Ran GTPase Q69L Ran (n=3 independent experiments). Data indicate that the treatment-induced nuclear translocation of NCOR2 is Ran-dependent. **e**, Inhibiting NCOR2 nuclear translocation by expressing the Ran (Q69L) mutant sensitizes HMT-3522 T4–2 cell spheroids to TRAIL-induced apoptosis (n=3 independent experiments). **f**, The location of the nuclear localization signal (NLS; amino acids 680–685) of NCOR2. **g**, Immunofluorescence images showing that the NLS-deficient NCOR2 mutant (NCOR2 ΔNLS) fails to translocate into the cell nucleus in response to TRAIL treatment. Scale bar, 20 μm. Right: Overexpression (OE) of NCOR2 ΔNLS hypersensitizes HMT-3522 T4–2 cell spheroids to TRAIL (n=2–5 independent experiments, the exact n are provided in the numerical source data). Data are presented as mean ± s.e.m. (**a–e,g**). *P < 0.05; **P < 0.01; ***P < 0.001 compared to vehicle (**a**,**b**,**d**), cytoplasmic NCOR2 (**c**), vector (**e**), or NCOR2 OE (**g**), two-tailed unpaired Student's t-test.

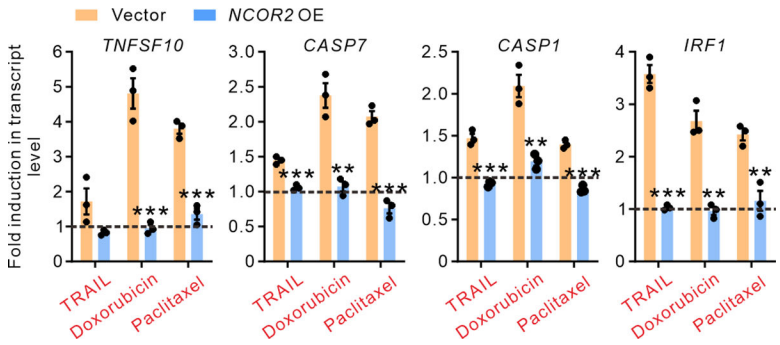

Extended Data Fig. 5. NCOR2 represses programmed cell death gene expression in breast cancer cells

Bar graphs showing fold expression of *TNFSF10* (encoding TRAIL), *CASP1* (encoding caspase 1), *CASP7* (encoding caspase 7), and *IRF1* (encoding IRF1) gene transcripts, in triple-negative breast cancer MDA-MB-231 cells with and without stable overexpression (OE) of *NCOR2* or an empty vector (Vector) following treatment with TRAIL (0.5 μg/ml × 3–12 hr), doxorubicin (1 μM × 24 hr), or paclitaxel (0.5 μM × 24 hr). The cells were co-treated with caspase inhibitors to avoid apoptosis and losing cells during RNA collection. Data are presented as mean ± s.e.m. (n=3 independent experiments). **P < 0.01; ***P < 0.001 compared to vector, two-tailed unpaired Student's t-test.

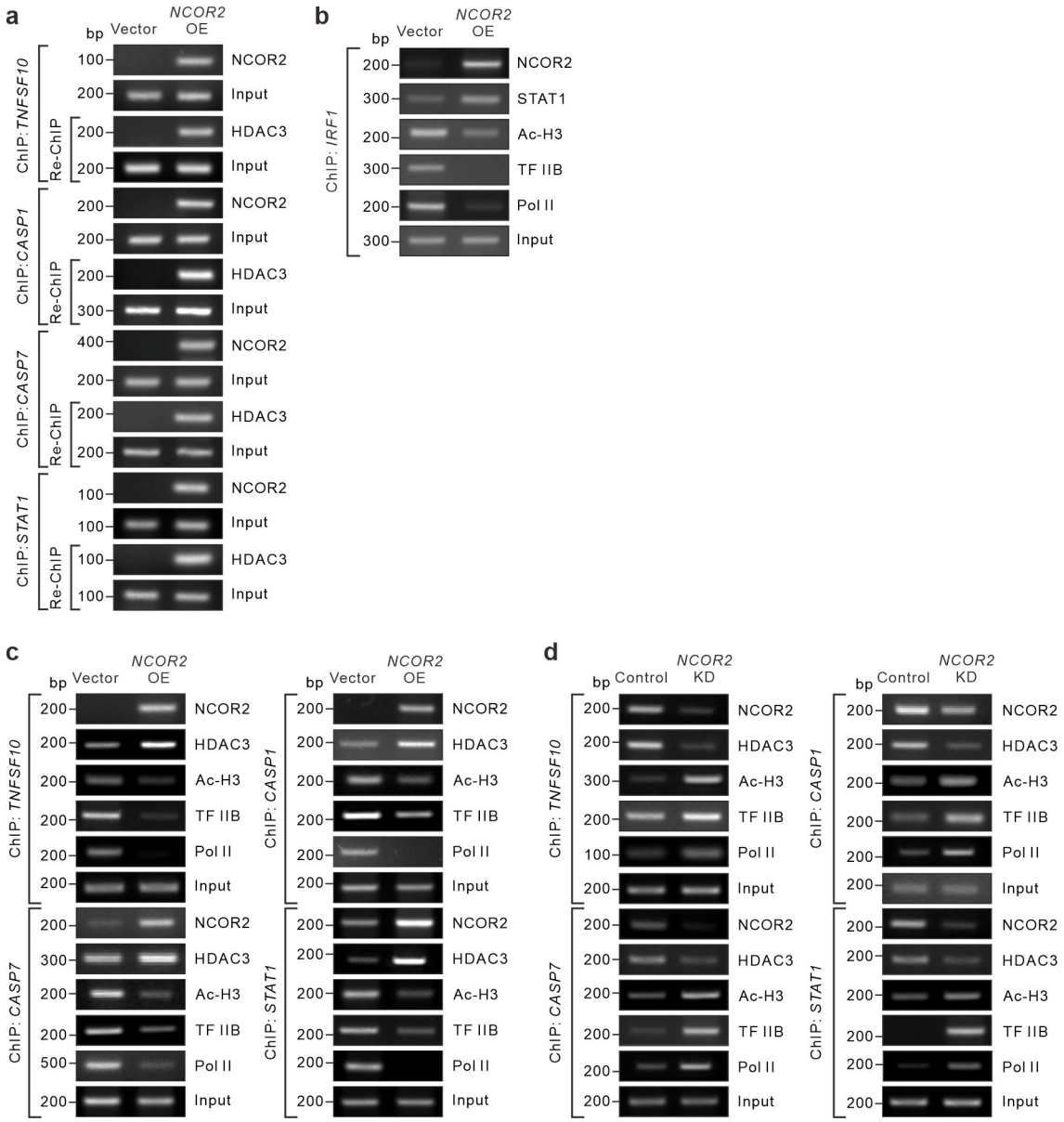

Extended Data Fig. 6. NCOR2 associates with the promoters of the genes in the STAT-1/IRF1 death signaling pathway

a, Results of chromatin immunoprecipitation (ChIP) and ChIP-re-ChIP assays showing that NCOR2 and HDAC3 are concomitantly recruited to the IRF1 binding site (IRF-E) at the *TNFSF10*, *CASP1*, *CASP7* or *STAT1* promoters in TRAIL (1 μg/mL × 3 hr)-treated HMT-3522 T4–2 cells overexpressing (OE) *NCOR2* or an empty vector (Vector). Re-ChIP was then carried out using the precipitates from the first round of ChIP for the indicated genes using anti-HDAC3 antibody (representative data of n=2 independent experiments with similar results). **b**, ChIP assay data showing association of NCOR2 together with STAT-1 at the *IRF1* promoter in TRAIL-treated HMT-3522 T4–2 cells with the OE of *NCOR2* or an empty vector (Vector) using anti-NCOR2, STAT-1, acetylated histone H3 (Ac-H3), transcription factor IIB (TF IIB), RNA polymerase II (Pol II) antibodies or an isotype

control IgG (representative data of n=2 independent experiments with similar results). **c**, ChIP assay data showing molecular associations of NCOR2 at the promoters of *TNFSF10*, *CASP1*, *CASP7* or *STAT1* in TRAIL-treated HMT-3522 T4–2 cells with the OE of *NCOR2* or an empty vector (Vector) using anti-NCOR2, HDAC3, Ac-H3, TF IIB, Pol II antibodies or an isotype control IgG (representative data of n=2 independent experiments with similar results). *d*, Results of ChIP from HMT-3522 T4–2 cells with lentiviral-shRNA-mediated knockdown (KD) of *NCOR2* expression showing attenuation of the association of HDAC3 with the IRF-E on the promoter of *TNFSF10*, *CASP1*, *CASP7* or *STAT1* following TRAIL treatment. Findings also showed that loss of NCOR2 simultaneously permitted histone hyperacetylation and enhanced the recruitment of the TF IIB and Pol II (representative data of n=2 independent experiments with similar results).

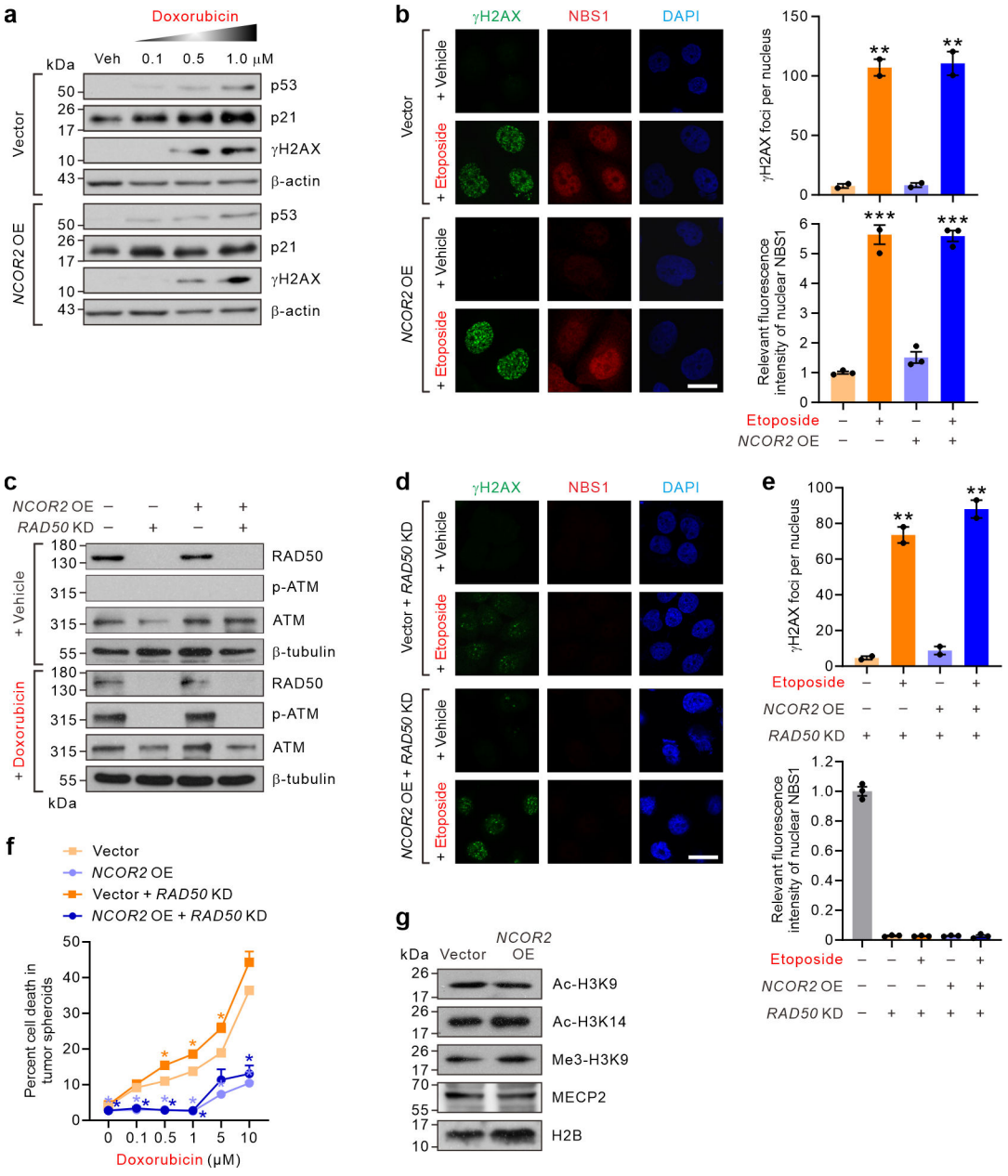

Extended Data Fig. 7. Overexpressing *NCOR2* does not interfere with DNA-damage signaling nor grossly alter chromatin conformation

a, p53, p21 and phosphorylated histone H2AX (γH2AX) in HMT-3522 T4–2 cells overexpressing *NCOR2* (*NCOR2* OE) compared to vector-infected cells treated with doxorubicin or vehicle (Veh) for 24 hr (representative data of n=2 independent experiments with similar results). **b**, Left: HMT-3522 T4–2 cells with *NCOR2* OE or infected with an empty vector (Vector) and treated with the DNA-damaging agent etoposide (5 μM × 2 hr) were stained for γH2AX and NBS-1. Scale, 20 μm. Right: The number of γH2AX nuclear foci (top; n=2 independent experiments) and the fluorescence intensity of nuclear NBS-1 per cell (bottom; n=3 independent experiments). **c**, RAD50, ATM, and phospho-ATM (S1981; p-ATM) in vehicle or doxorubicin-treated HMT-3522 T4–2 cells

with *NCOR2* OE or infected with an empty vector and with or without shRNA-mediated knockdown (KD) of *RAD50* expression (representative data of $n=2$ independent experiments with similar results). Loss of *RAD50* expression compromises DNA repair regardless of *NCOR2* expression. **d**, Immunofluorescence staining of γH2AX and NBS1 in HMT-3522 T4–2 cells overexpression *NCOR2* or infected with an empty vector with KD of *RAD50* expression treated with etoposide. Scale bar, 20 μm. Loss of *RAD50* expression abrogates DNA double strand break complex formation independent of cellular NCOR2 status. **e**, The number of γH2AX foci per cell nucleus (top; $n=2$ independent experiments) and the fluorescence intensity of nuclear NBS1 staining (bottom; $n=3$ independent experiments) in the cells shown in *d*. *f*, The percent cell death of HMT-3522 T4–2 cell spheroids treated with doxorubicin when they overexpressed *NCOR2* or an empty vector and when *RAD50* is knocked down. The OE of *NCOR2* was able to override the impact of loss of *RAD50* expression on cell death induction following doxorubicin treatment ($n=3$ independent experiments). *g*, Total nuclear acetylated (Ac)-histone-3 lysine-9 (Ac-H3K9), Ac-H3K14, trimethylated H3K9 (Me3-H3K9) and methyl-CpG binding protein 2 (MECP2) in HMT-3522 T4–2 cells overexpressing *NCOR2* compared to vector infected cells (representative data of $n=2$ independent experiments with similar results). Data are presented as mean ± s.e.m. (**b**,**e**,**f**). $*P < 0.05$; $**P < 0.01$; $***P < 0.001$ *versus* vehicle (**b**,**e**); $*P < 0.05$ *versus* vector (**f**), two-tailed unpaired Student's *t*-test.

Supplementary Material

Refer to Web version on PubMed Central for supplementary material.

Acknowledgements

We thank G. Timblin for constructive suggestions regarding interpretation of impact of NCOR2 on anti-tumor immunity, B. Welm (Huntsman Cancer Institute) and M. Lewis (Baylor College of Medicine) for the patient derived organoids, M. Lazar (University of Pennsylvania) for the monoclonal anti-NCOR2-producing hydridoma cell line and pcDNA-NCOR2 shRNA and mutant NCOR2 expression constructs, J. Park (Sungkyunkwan University) for the pcDNA3-IRF1 vector, C. Li for statistical analysis, and K. Tan for breast cancer tissues (Tung's Metro-Harbor Hospital). The cell culture, functional, and molecular studies were supported by grants from the NIH (R35-CA242447-01A1, R01-CA192914, and CA222508-01 to V.M.W), the DOD (BC122990 to V.M.W.), the BCRF (A132292 to V.M.W.). The development of the DeCOR2 gene therapy was funded by Taipei Medical University (107TMU-WFH-16, and 110-5433-001-400 to K.K.T.).

Main References

1. Szakacs G, Paterson JK, Ludwig JA, Booth-Genthe C & Gottesman MM Targeting multidrug resistance in cancer. Nat Rev Drug Discov 5, 219–234 (2006). [PubMed: 16518375]
2. Degterev A & Yuan J Expansion and evolution of cell death programmes. Nat Rev Mol Cell Biol 9, 378–390 (2008). [PubMed: 18414491]
3. Dikic I & Elazar Z Mechanism and medical implications of mammalian autophagy. Nat Rev Mol Cell Biol 19, 349–364 (2018). [PubMed: 29618831]
4. Holohan C, Van Schaeybroeck S, Longley DB & Johnston PG Cancer drug resistance: an evolving paradigm. Nat Rev Cancer 13, 714–726 (2013). [PubMed: 24060863]
5. Ayers M, et al. IFN-gamma-related mRNA profile predicts clinical response to PD-1 blockade. J Clin Invest 127, 2930–2940 (2017). [PubMed: 28650338]
6. Gao J, et al. Loss of IFN-gamma Pathway Genes in Tumor Cells as a Mechanism of Resistance to Anti-CTLA-4 Therapy. Cell 167, 397–404 e399 (2016). [PubMed: 27667683]

7. Manguso RT, et al. In vivo CRISPR screening identifies Ptpn2 as a cancer immunotherapy target. Nature 547, 413–418 (2017). [PubMed: 28723893]
8. Pan D, et al. A major chromatin regulator determines resistance of tumor cells to T cell-mediated killing. Science 359, 770–775 (2018). [PubMed: 29301958]
9. Rich JN & Bao S Chemotherapy and cancer stem cells. Cell Stem Cell 1, 353–355 (2007). [PubMed: 18371369]
10. Zitvogel L, Galluzzi L, Smyth MJ & Kroemer G Mechanism of action of conventional and targeted anticancer therapies: reinstating immunosurveillance. Immunity 39, 74–88 (2013). [PubMed: 23890065]
11. Sistigu A, et al. Cancer cell-autonomous contribution of type I interferon signaling to the efficacy of chemotherapy. Nat Med 20, 1301–1309 (2014). [PubMed: 25344738]
12. Yum S, Li M & Chen ZJ Old dogs, new trick: classic cancer therapies activate cGAS. Cell research 30, 639–648 (2020). [PubMed: 32541866]
13. Zitvogel L, Galluzzi L, Kepp O, Smyth MJ & Kroemer G Type I interferons in anticancer immunity. Nat Rev Immunol 15, 405–414 (2015). [PubMed: 26027717]
14. Bidwell BN, et al. Silencing of Irf7 pathways in breast cancer cells promotes bone metastasis through immune escape. Nat Med 18, 1224–1231 (2012). [PubMed: 22820642]
15. Nathan C Points of control in inflammation. Nature 420, 846–852 (2002). [PubMed: 12490957]
16. Yoshimura A, Naka T & Kubo M SOCS proteins, cytokine signalling and immune regulation. Nat Rev Immunol 7, 454–465 (2007). [PubMed: 17525754]
17. Pardoll DM The blockade of immune checkpoints in cancer immunotherapy. Nat Rev Cancer 12, 252–264 (2012). [PubMed: 22437870]
18. Topalian SL, Drake CG & Pardoll DM Immune checkpoint blockade: a common denominator approach to cancer therapy. Cancer Cell 27, 450–461 (2015). [PubMed: 25858804]
19. Xing Y, Wang X, Jameson SC & Hogquist KA Late stages of T cell maturation in the thymus involve NF-kappaB and tonic type I interferon signaling. Nat Immunol 17, 565–573 (2016). [PubMed: 27043411]
20. DeRose YS, et al. Patient-derived models of human breast cancer: protocols for in vitro and in vivo applications in tumor biology and translational medicine. Curr Protoc Pharmacol Chapter 14, Unit14 23 (2013).
21. Nagle PW, Plukker JTM, Muijs CT, van Luijk P & Coppes RP Patient-derived tumor organoids for prediction of cancer treatment response. Semin Cancer Biol 53, 258–264 (2018). [PubMed: 29966678]
22. Zhang XM, et al. A Renewable Tissue Resource of Phenotypically Stable, Biologically and Ethnically Diverse, Patient-Derived Human Breast Cancer Xenograft Models. Cancer Research 73, 4885–4897 (2013). [PubMed: 23737486]
23. Weaver VM, et al. beta4 integrin-dependent formation of polarized three-dimensional architecture confers resistance to apoptosis in normal and malignant mammary epithelium. Cancer Cell 2, 205–216 (2002). [PubMed: 12242153]
24. Bruna A, et al. A Biobank of Breast Cancer Explants with Preserved Intra-tumor Heterogeneity to Screen Anticancer Compounds. Cell 167, 260-+ (2016). [PubMed: 27641504]
25. DeRose YS, et al. Tumor grafts derived from women with breast cancer authentically reflect tumor pathology, growth, metastasis and disease outcomes. Nature Medicine 17, 1514–U1227 (2011).
26. von Karstedt S, Montinaro A & Walczak H Exploring the TRAILs less travelled: TRAIL in cancer biology and therapy. Nat Rev Cancer 17, 352–366 (2017). [PubMed: 28536452]
27. Pizzoferrato E, et al. Ectopic expression of interferon regulatory factor-1 promotes human breast cancer cell death and results in reduced expression of survivin. Cancer Res 64, 8381–8388 (2004). [PubMed: 15548708]
28. Clarke N, Jimenez-Lara AM, Voltz E & Gronemeyer H Tumor suppressor IRF-1 mediates retinoid and interferon anticancer signaling to death ligand TRAIL. EMBO J 23, 3051–3060 (2004). [PubMed: 15241475]

29. Stang MT, et al. Interferon regulatory factor-1-induced apoptosis mediated by a ligand-independent fas-associated death domain pathway in breast cancer cells. Oncogene 26, 6420–6430 (2007). [PubMed: 17452973]
30. Ciaccio MF, Wagner JP, Chuu CP, Lauffenburger DA & Jones RB Systems analysis of EGF receptor signaling dynamics with microwestern arrays. Nat Methods 7, 148–155 (2010). [PubMed: 20101245]
31. Codina A, et al. Structural insights into the interaction and activation of histone deacetylase 3 by nuclear receptor corepressors. Proc Natl Acad Sci U S A 102, 6009–6014 (2005). [PubMed: 15837933]
32. Guenther MG, Barak O & Lazar MA The SMRT and N-CoR corepressors are activating cofactors for histone deacetylase 3. Mol Cell Biol 21, 6091–6101 (2001). [PubMed: 11509652]
33. Litvak V, et al. A FOXO3-IRF7 gene regulatory circuit limits inflammatory sequelae of antiviral responses. Nature 490, 421–425 (2012). [PubMed: 22982991]
34. Esserman LJ, et al. Pathologic complete response predicts recurrence-free survival more effectively by cancer subset: results from the I-SPY 1 TRIAL--CALGB 150007/150012, ACRIN 6657. J Clin Oncol 30, 3242–3249 (2012). [PubMed: 22649152]
35. Chang JC, et al. Gene expression profiling for the prediction of therapeutic response to docetaxel in patients with breast cancer. Lancet 362, 362–369 (2003). [PubMed: 12907009]
36. Modlich O, Prisack HB, Munnes M, Audretsch W & Bojar H Predictors of primary breast cancers responsiveness to preoperative epirubicin/cyclophosphamide-based chemotherapy: translation of microarray data into clinically useful predictive signatures. J Transl Med 3, 32 (2005). [PubMed: 16091131]
37. van de Vijver MJ, et al. A gene-expression signature as a predictor of survival in breast cancer. N Engl J Med 347, 1999–2009 (2002). [PubMed: 12490681]
38. Gyorffy B, et al. An online survival analysis tool to rapidly assess the effect of 22,277 genes on breast cancer prognosis using microarray data of 1,809 patients. Breast Cancer Res Treat 123, 725–731 (2010). [PubMed: 20020197]
39. Liedtke C, et al. Response to neoadjuvant therapy and long-term survival in patients with triple-negative breast cancer. J Clin Oncol 26, 1275–1281 (2008). [PubMed: 18250347]
40. You SH, et al. Nuclear receptor co-repressors are required for the histone-deacetylase activity of HDAC3 in vivo. Nat Struct Mol Biol 20, 182–187 (2013). [PubMed: 23292142]
41. Li J, et al. Both corepressor proteins SMRT and N-CoR exist in large protein complexes containing HDAC3. EMBO J 19, 4342–4350 (2000). [PubMed: 10944117]
42. Bouker KB, et al. Interferon regulatory factor-1 (IRF-1) exhibits tumor suppressor activities in breast cancer associated with caspase activation and induction of apoptosis. Carcinogenesis 26, 1527–1535 (2005). [PubMed: 15878912]
43. Bourgeois-Daigneault MC, et al. Neoadjuvant oncolytic virotherapy before surgery sensitizes triple-negative breast cancer to immune checkpoint therapy. Sci Transl Med 10(2018).
44. Grimm D, et al. In vitro and in vivo gene therapy vector evolution via multispecies interbreeding and retargeting of adeno-associated viruses. J Virol 82, 5887–5911 (2008). [PubMed: 18400866]
45. Quezada SA, Peggs KS, Curran MA & Allison JP CTLA4 blockade and GM-CSF combination immunotherapy alters the intratumor balance of effector and regulatory T cells. J Clin Invest 116, 1935–1945 (2006). [PubMed: 16778987]
46. Schmid P, Dent R & O'Shaughnessy J Pembrolizumab for Early Triple-Negative Breast Cancer Reply. New Engl J Med 382(2020).
47. Savas P, et al. Clinical relevance of host immunity in breast cancer: from TILs to the clinic. Nat Rev Clin Oncol 13, 228–241 (2016). [PubMed: 26667975]
48. Yan Q, et al. Nuclear factor-kappaB binding motifs specify Toll-like receptor-induced gene repression through an inducible repressosome. Proc Natl Acad Sci U S A 109, 14140–14145 (2012). [PubMed: 22891325]
49. Pan D, et al. A major chromatin regulator determines resistance of tumor cells to T cell-mediated killing. Science (2018).
50. Alenghat T, et al. Histone deacetylase 3 coordinates commensal-bacteria-dependent intestinal homeostasis. Nature 504, 153–157 (2013). [PubMed: 24185009]

51. Guarneri V, et al. Prognostic value of pathologic complete response after primary chemotherapy in relation to hormone receptor status and other factors. J Clin Oncol 24, 1037–1044 (2006). [PubMed: 16505422]
52. Nanda R, et al. Pembrolizumab in Patients With Advanced Triple-Negative Breast Cancer: Phase Ib KEYNOTE-012 Study. J Clin Oncol 34, 2460–2467 (2016). [PubMed: 27138582]
53. Jiang Z, et al. Tucidinostat plus exemestane for postmenopausal patients with advanced, hormone receptor-positive breast cancer (ACE): a randomised, double-blind, placebo-controlled, phase 3 trial. Lancet Oncol 20, 806–815 (2019). [PubMed: 31036468]
54. Tuveson D & Clevers H Cancer modeling meets human organoid technology. Science 364, 952–955 (2019). [PubMed: 31171691]
55. Tiriac H, et al. Organoid Profiling Identifies Common Responders to Chemotherapy in Pancreatic Cancer. Cancer Discov 8, 1112–1129 (2018). [PubMed: 29853643]
56. Vlachogiannis G, et al. Patient-derived organoids model treatment response of metastatic gastrointestinal cancers. Science 359, 920–926 (2018). [PubMed: 29472484]
57. Weaver VM, et al. Reversion of the malignant phenotype of human breast cells in three-dimensional culture and in vivo by integrin blocking antibodies. J Cell Biol 137, 231–245 (1997). [PubMed: 9105051]
58. Drain AP, et al. Matrix compliance permits NF-kappaB activation to drive therapy resistance in breast cancer. J Exp Med 218(2021).
59. Chan TS, et al. Metronomic chemotherapy prevents therapy-induced stromal activation and induction of tumor-initiating cells. Journal of Experimental Medicine 213, 2967–2988 (2016). [PubMed: 27881732]
60. Britton S, Coates J & Jackson SP A new method for high-resolution imaging of Ku foci to decipher mechanisms of DNA double-strand break repair. J Cell Biol 202, 579–595 (2013). [PubMed: 23897892]
61. Ishizuka T & Lazar MA The N-CoR/histone deacetylase 3 complex is required for repression by thyroid hormone receptor. Mol Cell Biol 23, 5122–5131 (2003). [PubMed: 12861000]
62. Broutier L, et al. Culture and establishment of self-renewing human and mouse adult liver and pancreas 3D organoids and their genetic manipulation. Nature Protocols 11, 1724–1743 (2016). [PubMed: 27560176]
63. Park EJ, et al. SMRTe, a silencing mediator for retinoid and thyroid hormone receptors-extended isoform that is more related to the nuclear receptor corepressor. Proc Natl Acad Sci U S A 96, 3519–3524 (1999). [PubMed: 10097068]
64. Kinsella TM & Nolan GP Episomal vectors rapidly and stably produce high-titer recombinant retrovirus. Hum Gene Ther 7, 1405–1413 (1996). [PubMed: 8844199]
65. Gossen M & Bujard H Tight control of gene expression in mammalian cells by tetracycline-responsive promoters. Proc Natl Acad Sci U S A 89, 5547–5551 (1992). [PubMed: 1319065]
66. Park J, et al. Elevated level of SUMOylated IRF-1 in tumor cells interferes with IRF-1-mediated apoptosis. Proc Natl Acad Sci U S A 104, 17028–17033 (2007). [PubMed: 17942705]
67. Lee JL, Wang MJ & Chen JY Acetylation and activation of STAT3 mediated by nuclear translocation of CD44. J Cell Biol 185, 949–957 (2009). [PubMed: 19506034]
68. Ory DS, Neugeboren BA & Mulligan RC A stable human-derived packaging cell line for production of high titer retrovirus/vesicular stomatitis virus G pseudotypes. Proc Natl Acad Sci U S A 93, 11400–11406 (1996). [PubMed: 8876147]
69. Yu J, Li Y, Ishizuka T, Guenther MG & Lazar MA A SANT motif in the SMRT corepressor interprets the histone code and promotes histone deacetylation. EMBO J 22, 3403–3410 (2003). [PubMed: 12840002]
70. Dignam JD, Lebovitz RM & Roeder RG Accurate transcription initiation by RNA polymerase II in a soluble extract from isolated mammalian nuclei. Nucleic Acids Res 11, 1475–1489 (1983). [PubMed: 6828386]
71. Yu J, et al. Integrative genomics analysis reveals silencing of beta-adrenergic signaling by polycomb in prostate cancer. Cancer cell 12, 419–431 (2007). [PubMed: 17996646]
72. Lee GY, Kenny PA, Lee EH & Bissell MJ Three-dimensional culture models of normal and malignant breast epithelial cells. Nat Methods 4, 359–365 (2007). [PubMed: 17396127]

73. Ho Sui SJ, et al. oPOSSUM: identification of over-represented transcription factor binding sites in co-expressed genes. Nucleic Acids Res 33, 3154–3164 (2005). [PubMed: 15933209]

74. Chan TS, et al. Metronomic chemotherapy prevents therapy-induced stromal activation and induction of tumor-initiating cells. J Exp Med 213, 2967–2988 (2016). [PubMed: 27881732]

75. Bohning D, Boehning W & Holling H Revisiting youden's index as a useful measure of the misclassification error in meta-analysis of diagnostic studies. Stat Methods Med Res 17, 543–554 (2008). [PubMed: 18375457]

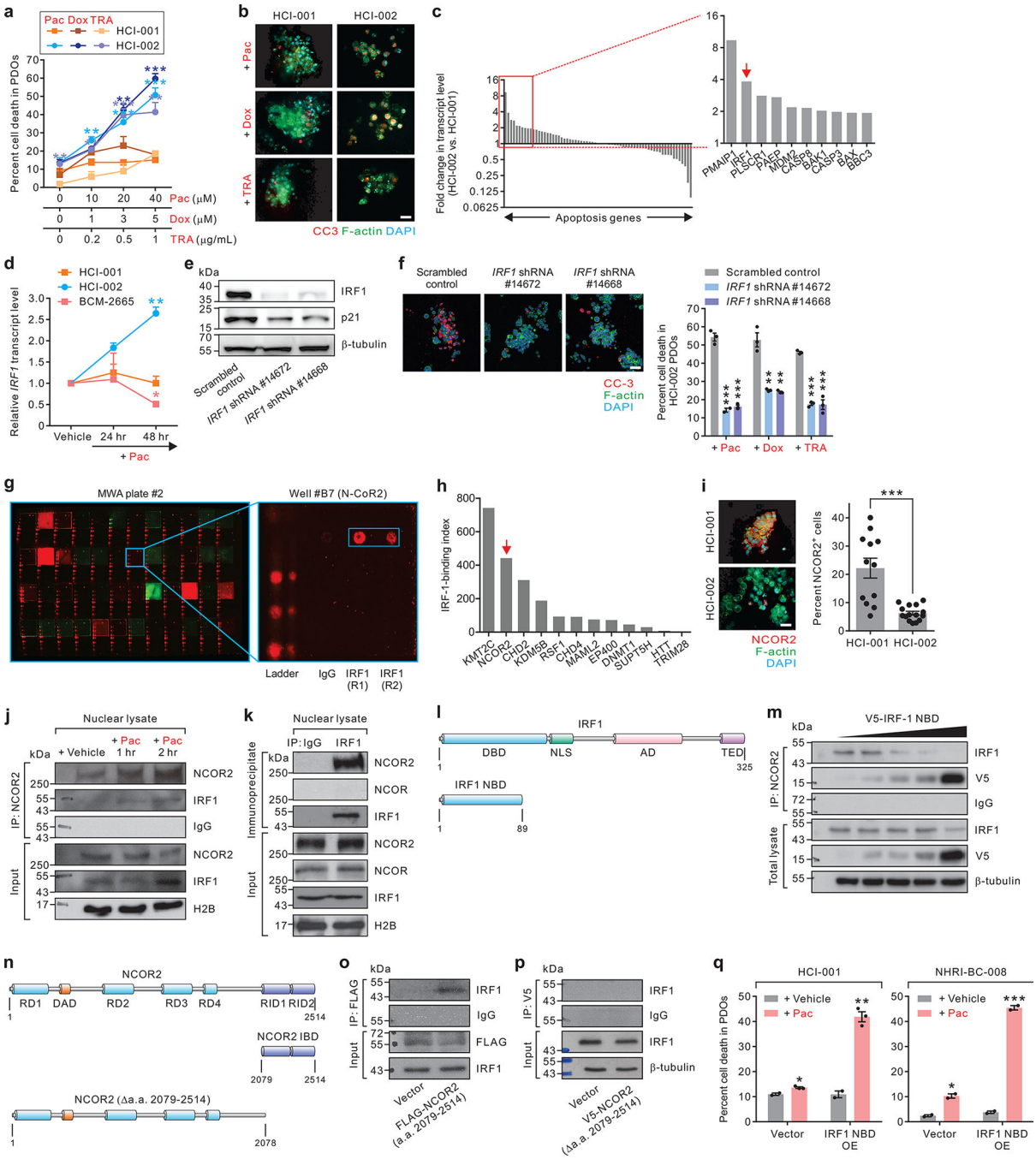

Fig. 1 |. Identification of NCOR2 as an IRF1 stress-dependent death regulator.

a, Line graphs showing percent cell death in HCI-001 or HCI-002 PDOs in response to increasing concentration of paclitaxel (Pac), doxorubicin (Dox) or TRAIL (TRA). Data are presented as mean ± s.e.m.; *n*=3–11 PDOs (the exact *n* are provided in the numerical source data). **b**, Representative confocal images of Pac (20 μM), Dox (5 μM), or TRA (1 μg/ml)-treated PDOs (n=*3* independent PDOs with similar results) immunostained for cleaved caspase 3 (CC3), F-actin, and 4′,6-diamidino-2-phenylindole (DAPI). Scale bar, 20 μm. **c**, *IRF1* as the top ranked apoptosis gene whose transcription was induced in

chemo-sensitive HCI-002 PDOs compared to chemo-resistant HCI-001 PDOs following treatment with Pac (20 μM × 48 hr) or vehicle as analyzed by RNA-sequencing (Methods; experiment was performed once). **d**, The transcript level of *IRF1* in Pac-treated PDOs as measured by qRT-PCR analysis (n=3 independent PDO culture experiments). **e**, The knockdown of *IRF1* expression in HCI-002 PDOs using lentivirus-mediated transduction of shRNAs (representative data of n=2 independent experiments with similar results). **f**, Confocal images of Pac, Dox or TRA-treated HCI-002 PDOs immunostained for CC3, F-actin, and DAPI. Scale bar, 20 μm. Right: Percent cell death in the treated PDOs (n=3 PDOs). **g**, Micro-Western Array (MWA) blots obtained from analyzing IgG (control) or IRF1 (experimental replicates; IRF1-R1 and IRF1-R2) immunoprecipitates from the nuclear lysate of TRAIL-treated HMT-3522 T4–2 cells. **h**, Bar graph depicting the IRF1-binding index calculated for nuclear proteins identified by the MWA analysis (Methods; experiment was performed once). **i**, Confocal images of treatment-resistant HCI-001 and treatment-sensitive HCI-002 PDOs immunostained for NCOR2, F-actin, and DAPI. Scale bar, 20 μm. Right: Bar graph showing percent cells with positive NCOR2 staining (n=12–15 PDOs, the exact n are provided in the numerical source data). **j**, Pac treatment enhances the interaction of NCOR2 with IRF1 in NHRI-BC-008 cells (representative data of n=2 independent experiments with similar results). **k**, IRF1 associates with NCOR2 but not its paralog NCOR in HMT-3522 T4–2 cells (representative data of n=2 independent experiments with similar results). **l**, The functional domains of IRF1 and the domain mediating its binding to NCOR2 (Extended Data Fig. 2). **m**, The NCOR2-binding domain (NBD) of IRF1 dose-dependently abrogates the interaction between endogenous IRF1 and NCOR2 (representative data of n=2 independent experiments with similar results). **n**, The functional domains of NCOR2 (Extended Data Fig. 2). **o**, The C-terminal region of NCOR2 (a.a. 2079–2514) interacts with IRF1 in MDA-MB-436 cells (representative data of n=2 independent experiments with similar results). **p**, The IRF1-binding domain (IBD)-deficient NCOR2 (Δa.a. 2079–2514) fails to interact with IRF1 (representative data of n=2 independent experiments with similar results). **q**, OE of the IRF1 NBD hypersensitizes breast cancer PDOs to Pac (10 μM × 24 hr)-induced cell death (n=3 PDOs). Data are presented as mean ± s.e.m. (**a**,**d**,**f**,**i**,**q**). *P < 0.05; **P < 0.01; ***P < 0.001 compared to HCI-001 (**a**,**d**,**i**), scrambled control (**f**), or vehicle (**q**); two-tailed unpaired Student's t-test.

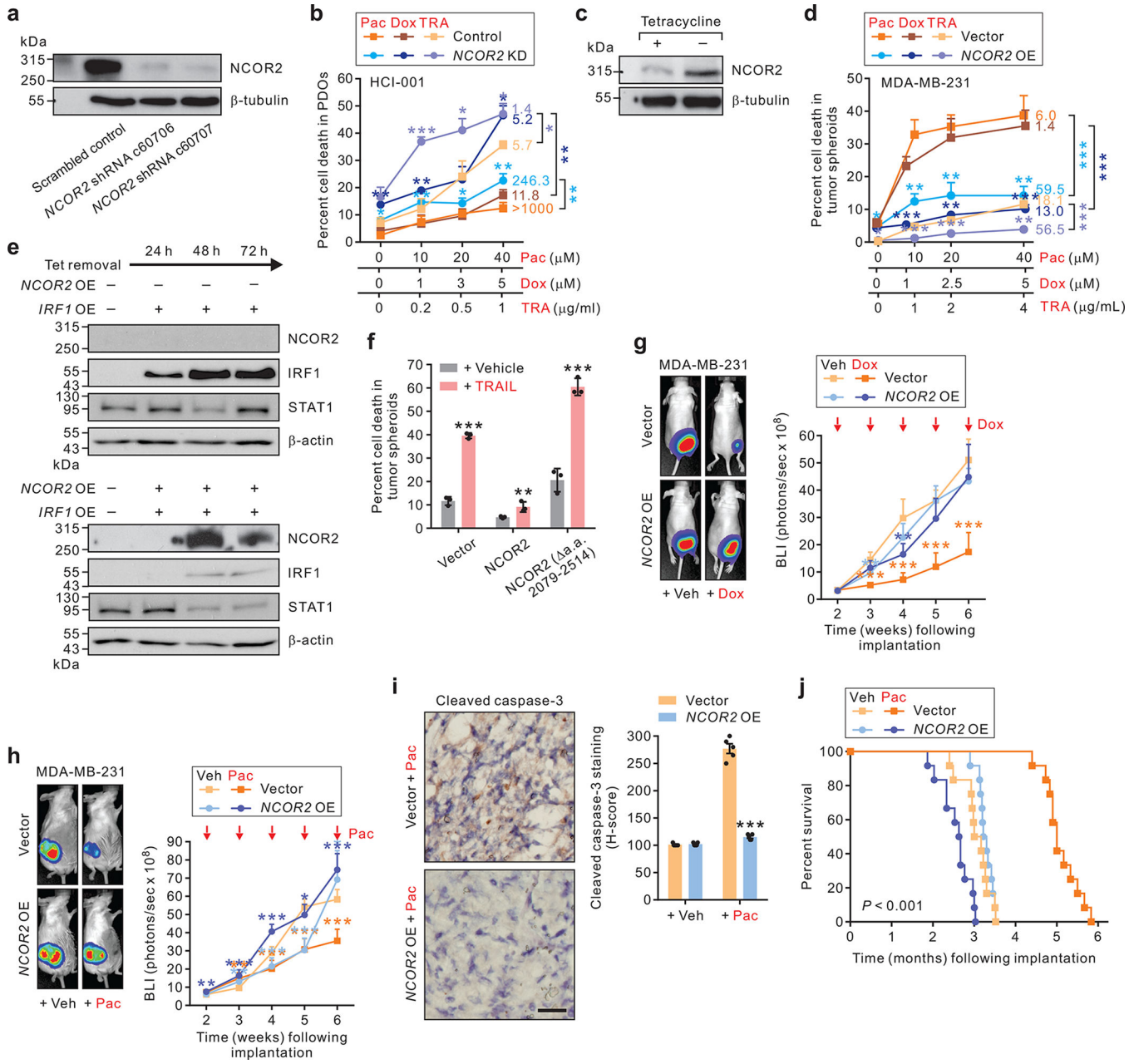

Fig. 2 |. NCOR2 modulates the innate death-resistance of breast cancers.

a, The KD of *NCOR2* expression in HCI-001 PDOs using lentivirus-mediated transduction of shRNAs (representative data of n=2 independent experiments with similar results). **b**, KD of *NCOR2* expression rendered HCI-001 PDOs hypersensitive to Pac, Dox, or TRA. Data are presented as mean ± s.e.m.; n=3 PDOs. Numbers associated with each line denote the 50% inhibitory concentrations (IC50). **c**, The protein abundance level of NCOR2 in MDA-MB-231 cells carrying a tetracycline (Tet)-regulated NCOR2 expression construct (representative data of n=2 independent experiments with similar results). **d**, MDA-MB-231 cell-derived tumor spheroids overexpressing *NCOR2* were less sensitive to treatment (n=3 independent experiments). Numbers associated with each line denote the 20% inhibitory

concentrations. **e**, The inducible OE of *NCOR2* represses transcriptional induction of IRF1 and STAT1 in HMT-3522 T4–2 cells stimulated to overexpress *IRF1* (representative data of n=2 independent experiments with similar results). **f**, The OE of the IRF1-binding domain-deficient NCOR2 (Δa.a. 2079–2514) hypersensitizes HMT-3522 T4–2 spheroids to TRAIL (n=3 spheroids per group). **g**,**h**, Representative bioluminescence images (BLI) of MDA-MB-231 xenografted tumors with and without *NCOR2* OE following systemic treatment with Dox (**g**), Pac (**h**) or vehicle (Veh). Right: The impact of increasing *NCOR2* expression on the size of MDA-MB-231 xenografted tumors following treatments (n=12 mice per group). **i**, Cleaved caspase-3 staining in xenografted MDA-MB-231 breast tumors with and without *NCOR2* OE following systemic treatment with Pac. Scale bar, 50 μm. Right: cleaved caspase-3 in tissues (n=5 tissue sections per group). Data are represented as mean ± s.e.m. (**b**,**d**,**f-i**). *P < 0.05; **P < 0.01; ***P < 0.001 compared to control shRNA (**b**), vector (**d**,**i**), vehicle (**f**), or vector *plus* vehicle (**g**,**h**), two-tailed unpaired Student's t-test or ordinary two-way ANOVA (**b**,**d**). **j**, Line graphs showing reduced survival of mice injected in the mammary fat pads with MDA-MD-231 breast cancer cells overexpressing *NCOR2* despite Pac treatments (n=12 mice per group). Statistical analysis was performed using the log-rank test.

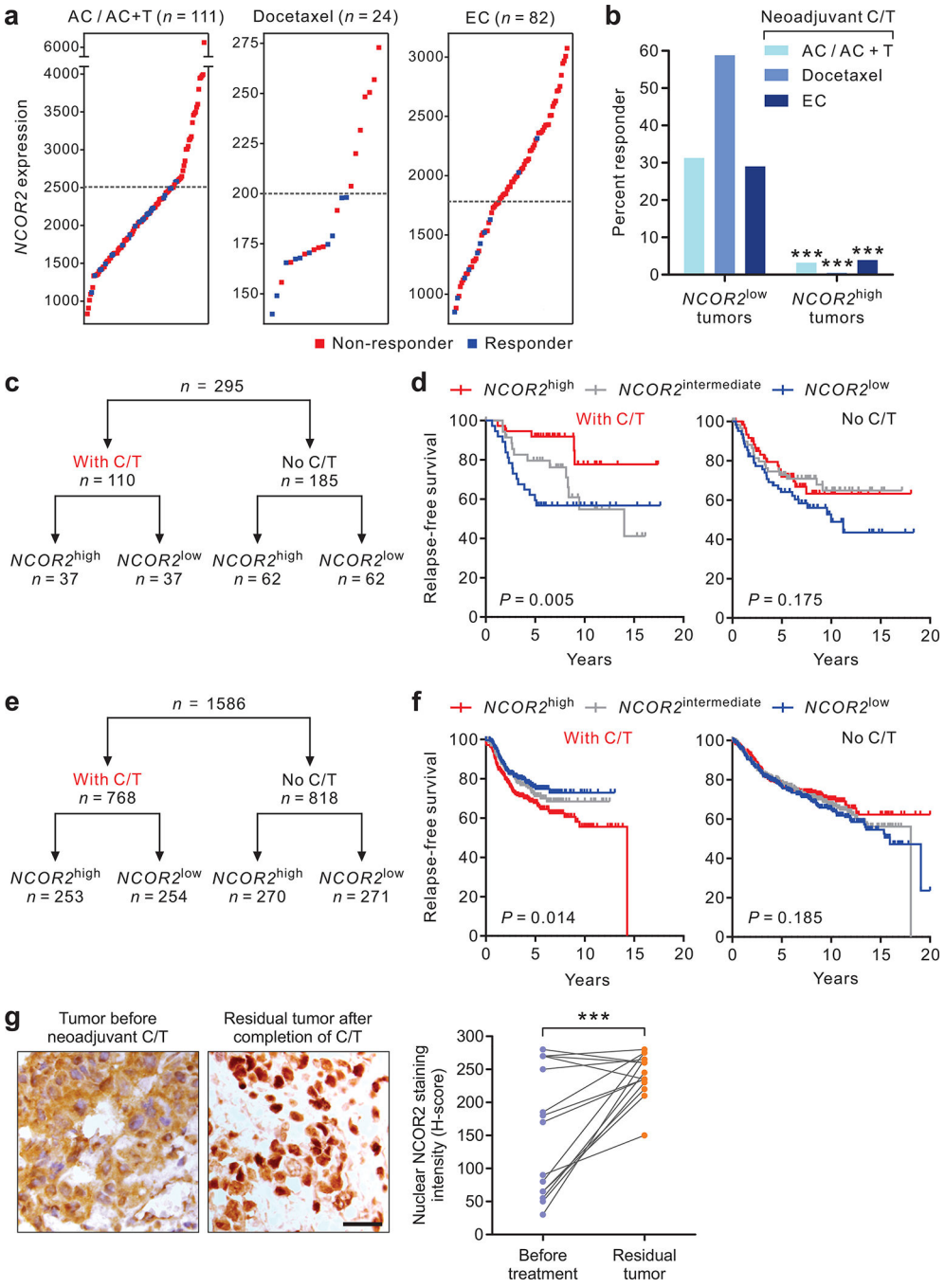

Fig. 3 |. NCOR2 expression correlates with chemo-resistance in human breast cancer.

a, *NCOR2* transcript levels of responsive and non-responsive breast cancers in patients receiving neoadjuvant chemotherapy (C/T) (Methods). AC, adriamycin plus cyclophosphamide; T, paclitaxel; EC, epirubicin plus cyclophosphamide. **b**, Bar graphs showing percentage of C/T responders in patients with high- or low-*NCOR2* levels in their primary breast cancer. $^{**}P < 0.01$; $^{***}P < 0.001$, two-sided Fisher's exact test (n=111, 24, and 82 patients in the respective data sets; Methods). **c**,**e**, Diagrams illustrating clinical analytical protocol for investigating the predictive value of *NCOR2* expression in

patients with breast cancer (Methods). **d**,**f**, Graphs showing relapse-free survival disparities in patients receiving adjuvant C/T or those not, based upon partitioning into tertiles by *NCOR2* expression status. The numbers of the patients included in each of the analyses are shown in **c** and **e**. Statistical analysis was performed using the two-sided log-rank test. **g**, Representative immunohistochemical images of NCOR2 staining of paired triple-negative breast cancer (TNBC) tissues before and after neoadjuvant C/T (n=15 tumors). Scale bar, 50 μm. Right: Line graphs quantifying the nuclear NCOR2 staining intensity of the stained TNBC tissue shown at left. ***$P < 0.001$, two-tailed unpaired Student's t-test.

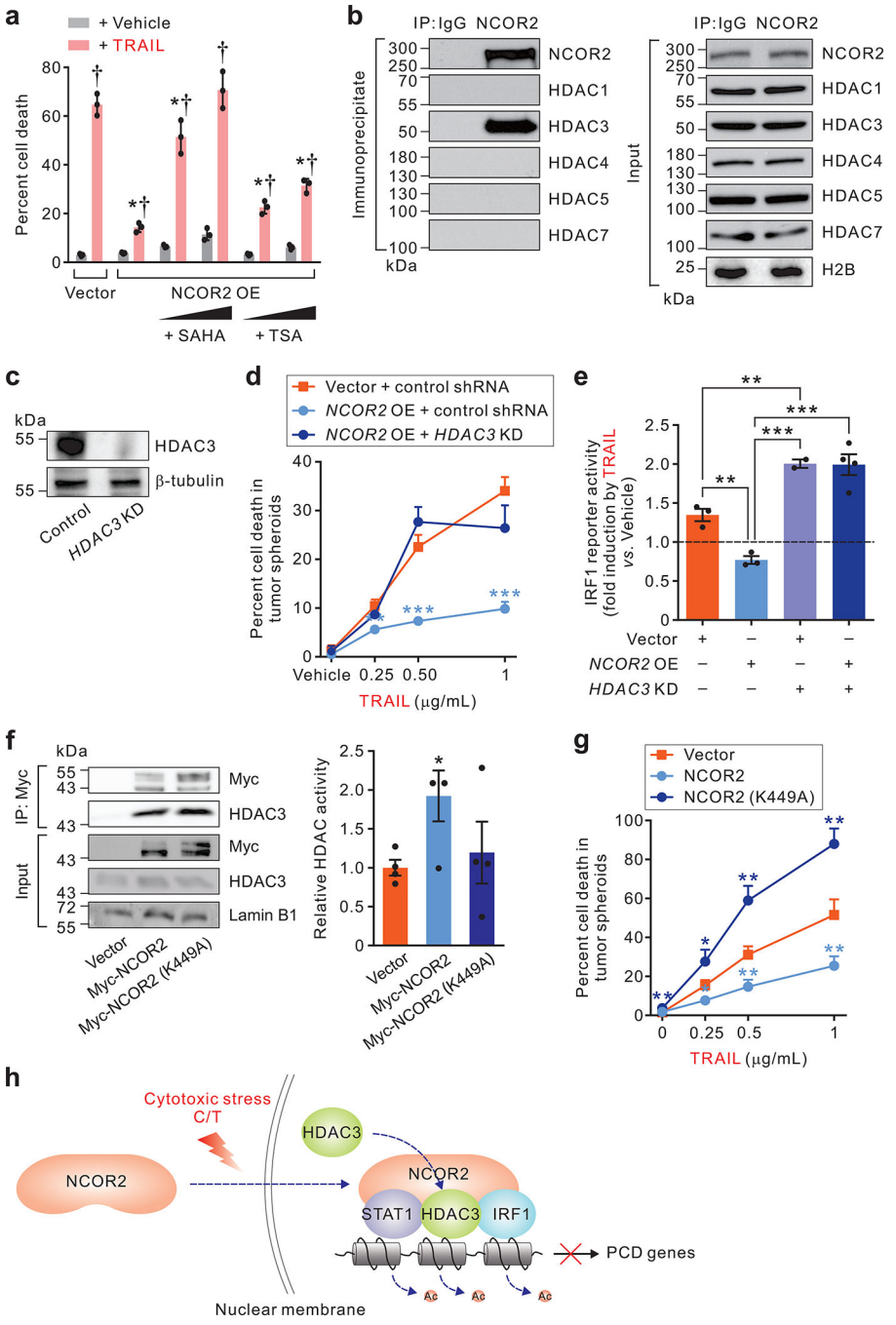

Fig. 4 |. The NCOR2 stress checkpoint is HDAC3-dependent.

a, Bar graphs showing the HDAC inhibitors (SAHA [1–5 μM] or TSA [0.1–0.5 μM]) restore the sensitivity of HMT-3522 T4–2 breast cancer cells overexpressing *NCOR2* or an empty vector to the cytotoxic stimuli TRAIL (1 μg/ml × 24 hr). Data are presented as mean ± s.e.m.; n=3 independent experiments. **b**, Representative immunoblot showing NCOR2 co-immunoprecipitates (IP) with HDAC3 in the nuclear lysates of TRAIL-treated HMT-3522 T4–2 cells (representative data of n=2 independent experiments with similar results). **c**, Representative immunoblots showing shRNA-mediated knockdown (KD) of

HDAC3 expression in HMT-3522 T4–2 cells (representative data of n=2 independent experiments with similar results). **d**, Line graphs showing knockdown (KD) of *HDAC3* expression restores the treatment-sensitivity of HMT-3522 T4–2 spheroids even when they overexpress (OE) *NCOR2* (n=3 independent experiments). **e**, Bar graphs showing the impact of *HDAC3* knockdown (KD) on TRAIL-induced IRF1 activity in HMT-3522 T4–2 cells with or without *NCOR2* overexpression (OE) (n=2–4 independent experiments, the exact n are provided in the numerical source data). **f**, A functionally deficient NCOR2 (K449A) mutant interacts specifically with HDAC3 to impede its nuclear deacetylase activity (n=4independent experiments). **g**, Forced expression of a mutant NCOR2 (K449A) but not wild-type NCOR2 hyper-sensitizes HMT-3522 T4–2 spheroids to cytotoxic-stress stimuli TRAIL (n=3 independent experiments). **h**, Cartoon showing cytotoxic stress and C/T induces the nuclear translocation of NCOR2, which recruits HDAC3 to the promoters of the IRF1 and/or STAT1 target genes, leading to promoter deacetylation and transcription repression of PCD genes in the treated tumor cells. Data are represented as mean ± s.e.m. (**a**,**d**-**g**). *P < 0.05 compared to vector plus TRAIL; †P < 0.05 compared to vehicle (**a**); *P < 0.05; **P < 0.01; ***P < 0.001 compared to vector (**d**,**e**,**f**, **g**), two-tailed unpaired Student's t-test.

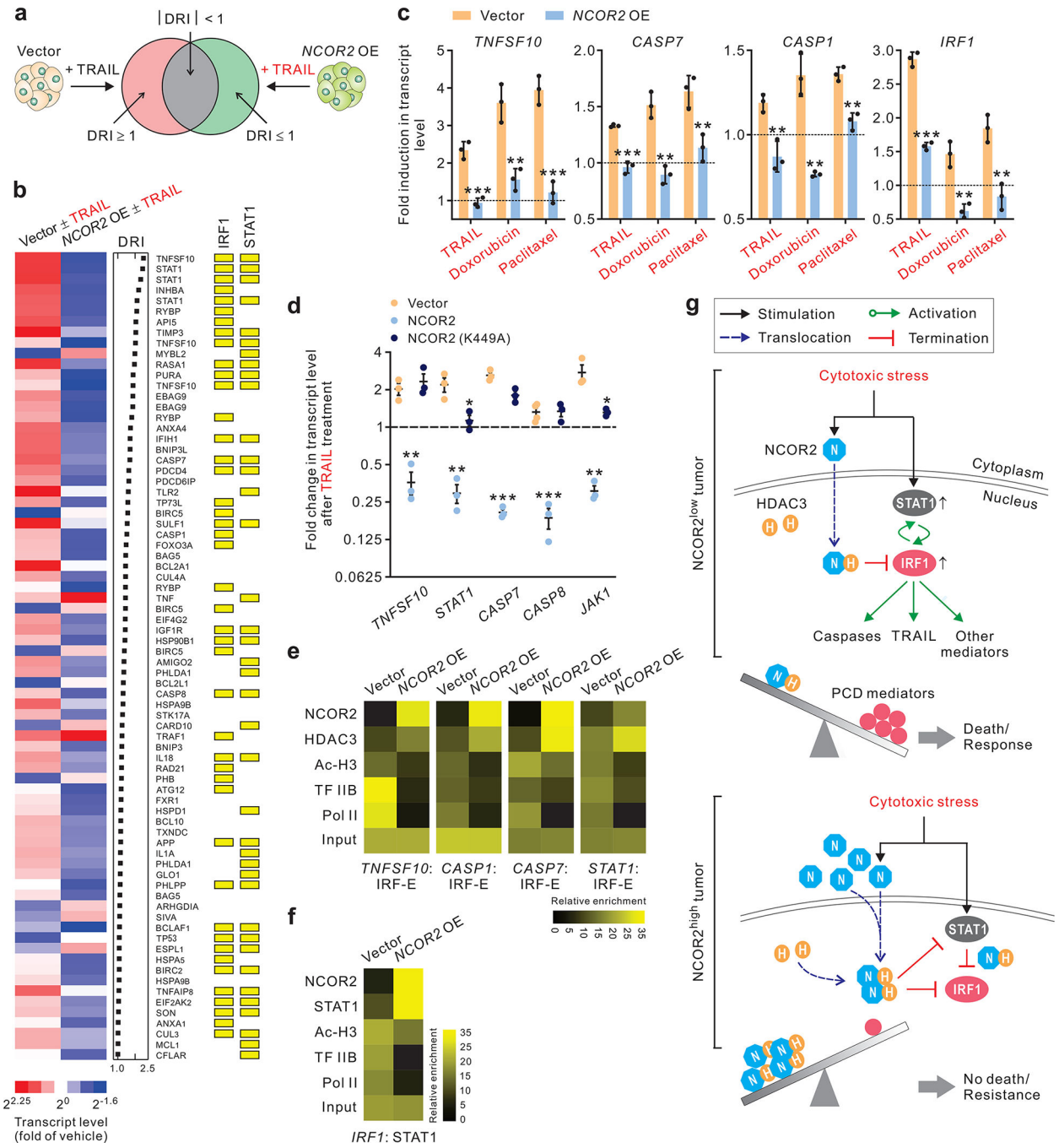

Fig. 5 |. NCOR2 is a chromatin-mediated checkpoint of STAT1/IRF1 stress signaling.

a, The strategy used to identify genes differentially responsive to TRAIL treatment in HMT-3522 T4–2 cells with or without OE of *NCOR2*. DRI, differential regulation index. **b**, Heat map showing the fold change in mean transcript level (on a $\log_2$ scale) of 64 NCOR2-related programmed cell death (PCD) genes in HMT-3522 T4–2 cells in response to treatment with TRAIL (1 μg/ml × 3 hr) without or with OE of *NCOR2*. The genes with IRF1 or STAT1 consensus binding sites in their promoter are highlighted in yellow. **c**, Bar graphs showing fold expression of *TNFSF10*, *CASP1*, *CASP7*, and *IRF1* gene transcript in

HMT-3522 T4–2 cells with and without *NCOR2* OE following treatment with TRAIL (1 μg/ml × 3–12 hr), doxorubicin (1 μM × 24 hr), or paclitaxel (0.5 μM × 24 hr) in the presence of caspase inhibitors. Data are presented as mean ± s.e.m.; n=3 independent experiments. **d**, Fold change in mRNA of selected PCD genes following TRAIL treatment normalized to vehicle control in HMT-3522 T4–2 cells either expressing an empty vector (vector), wild-type NCOR2 or the NCOR2 (K449A) mutant (n=3–4 independent experiments, the exact n are provided in the numerical source data). **e**, Heat map quantifying ChIP PCR assay results of the TRAIL-induced association of NCOR2 with the promoters of *TNFSF10*, *CASP1*, *CASP7* or *STAT1* together with HDAC3, concurrent histone hypoacetylation and reduced TF IIB and Pol II recruitment in HMT-3522 T4–2 cells with OE of *NCOR2* as compared to vector. **f**, A heat maps quantifying ChIP PCR assay results revealing how NCOR2 associates with STAT1 on the *IRF1* promoter and represses its transcription in TRAIL-treated HMT-3522 T4–2 cells without or with OE of *NCOR2*. **g**, Schematic model whereby following cytotoxic stress NCOR2 translocates into the nuclei of cells and recruits HDAC3 to attenuate STAT1-IRF1-induced PCD, to promote treatment-resistance in epithelial tumors. This stress and death checkpoint mechanism takes effect in tumors with high *NCOR2* expression ($NCOR2^{high}$), whereas it fails to protect cancer cells in $NCOR2^{low}$ tumors. Data are represented as mean ± s.e.m. (**c**,**d**). *P < 0.05; **P < 0.01; ***P < 0.001 compared to vector (**c**,**d**), two-tailed unpaired Student's t-test.

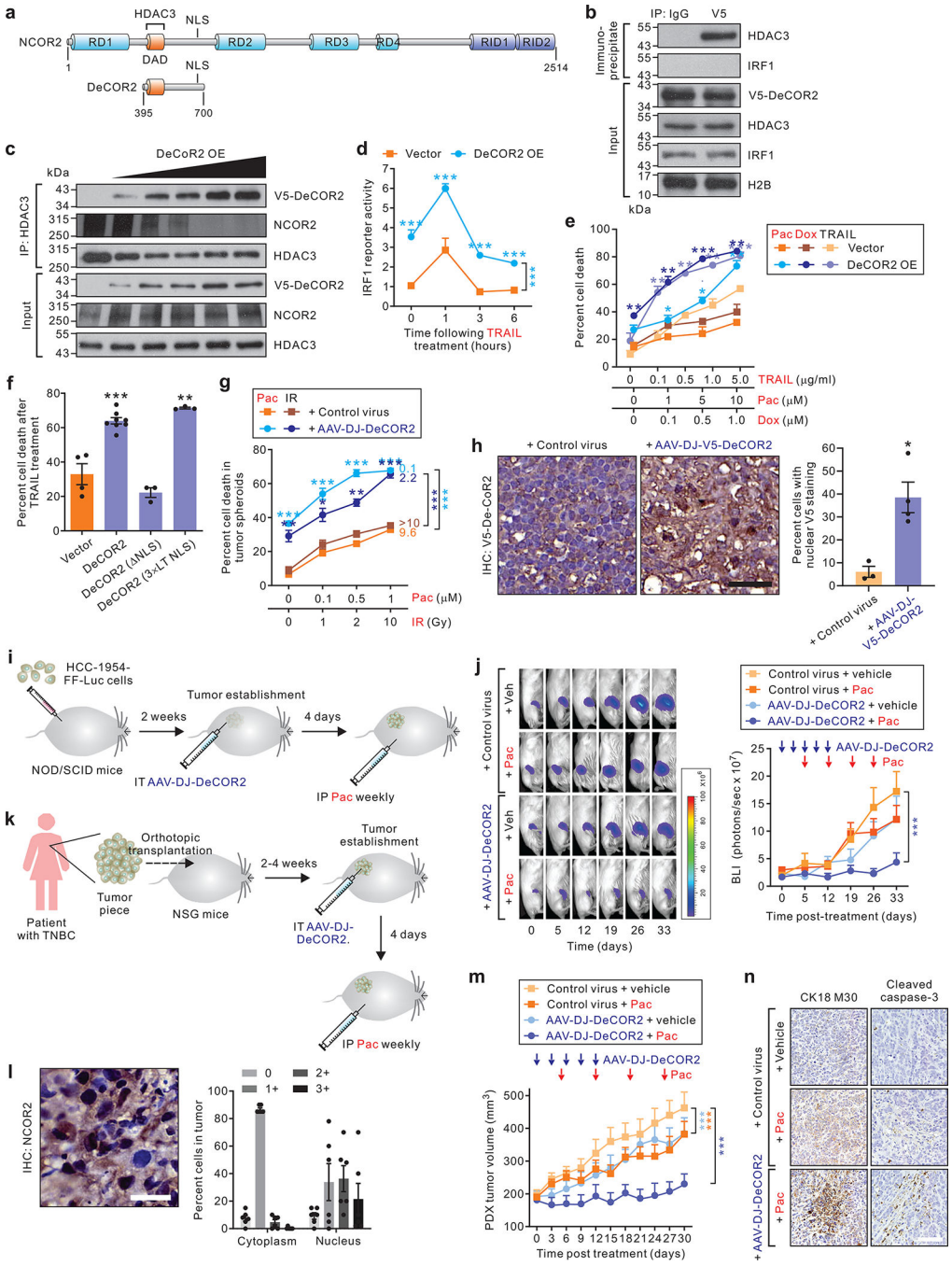

Fig. 6 |. Functionally blocking NCOR2 potentiates chemotherapy in breast tumors.

a, The functional domains of NCOR2 and the corresponding region on DeCOR2. **b**, V5-epitope-tagged DeCOR2 (V5-DeCOR2) interacts with HDAC3 but fails to interact with IRF1 in HCC-1954 cells (representative data of n=2 independent experiments with similar results). **c**, DeCOR2 competes with endogenous NCOR2 for the interaction with HDAC3. HCC-1954 cells were transfected with increasing amounts of V5-DeCOR2 and treated with TRAIL (1 μg/mL × 3 hr). The nuclear lysates were then subjected to co-IP (representative data of n=2 independent experiments with similar results). **d**, The transcriptional activity of

IRF1 in HCC-1954 cells with OE of DeCOR2 or an empty vector before and after treatment with TRAIL. Data are presented as mean ± s.e.m.; n=4 independent experiments. **e**, Percent cell death in HCC-1954 cells with OE of DeCOR2 or an empty vector after treatment with increasing concentrations of TRAIL, paclitaxel (Pac), or doxorubicin (Dox) (n=3 independent experiments). **f**, Percent cell death in HCC-1954 cells overexpressing DeCOR2, DeCOR2 (ΔNLS), DeCOR2 (3×LT NLS) or an empty vector following treatment with TRAIL (n=3–8 independent experiments, the exact n are provided in the numerical source data). **g**, Percent cell death in HCC-1954 spheroids infected with AAV-DJ-V5-DeCOR2 or control virus before and after treatment with increasing concentrations of Pac or increasing doses of ionizing radiation (IR) (n=3 independent experiments). Numbers associated with each line denote the 20% inhibitory concentrations. **h**, Immunohistochemical (IHC) staining for V5-epitope-tagged DeCOR2 of a xenografted orthotopic HCC-1954 tumor treated with intra-tumoral (IT) AAV-DJ-V5-DeCOR2 gene therapy or the control AAV. Scale bar, 25 μm. Right, The percentage of tumors cells expressing nuclear V5-epitope-tagged DeCOR2 (n=3 tumors per group). **i,** The AAV-DJ-DeCOR2 gene therapy strategy used to treat an orthotopic murine model of breast cancer. **j**, Bioluminescence images (BLI) of the mice treated as described in **i** and tumor bulk quantified as BLI normalized photon counts as a function of time (right) (n=10 mice per group). **k**, The AAV-DJ-DeCOR2 gene therapy strategy used to treat a PDX orthotopic model of TNBC (Methods). **l**, IHC image of NCOR2 staining of the human TNBC PDX tumor used in **k** before treatment. Scale bar, 25 μm. Right, The subcellular distribution of NCOR2 in cancer cells (n=6 tumors). **m**, The volume of the orthotopic human PDX tumors treated as in **k** (n=10 mice per group). **n**, IHC staining for the apoptosis markers cleaved caspase-3 and cytokeratin-18 neoepitope M30 (CK18 M30) in the treated PDX tumors depicted in **k**. Scale bar, 100 μm. Data are represented as mean ± s.e.m. (**d-h**,**j**,**l**,**m**). *P < 0.05; **P < 0.01; ***P < 0.001 compared to vector (**d-f**), control virus (**g**, **h**), or control virus + vehicle (**j**,**m**), two-tailed unpaired Student's t-test, or ordinary two-way ANOVA (**d**,**g**,**j**,**m**).

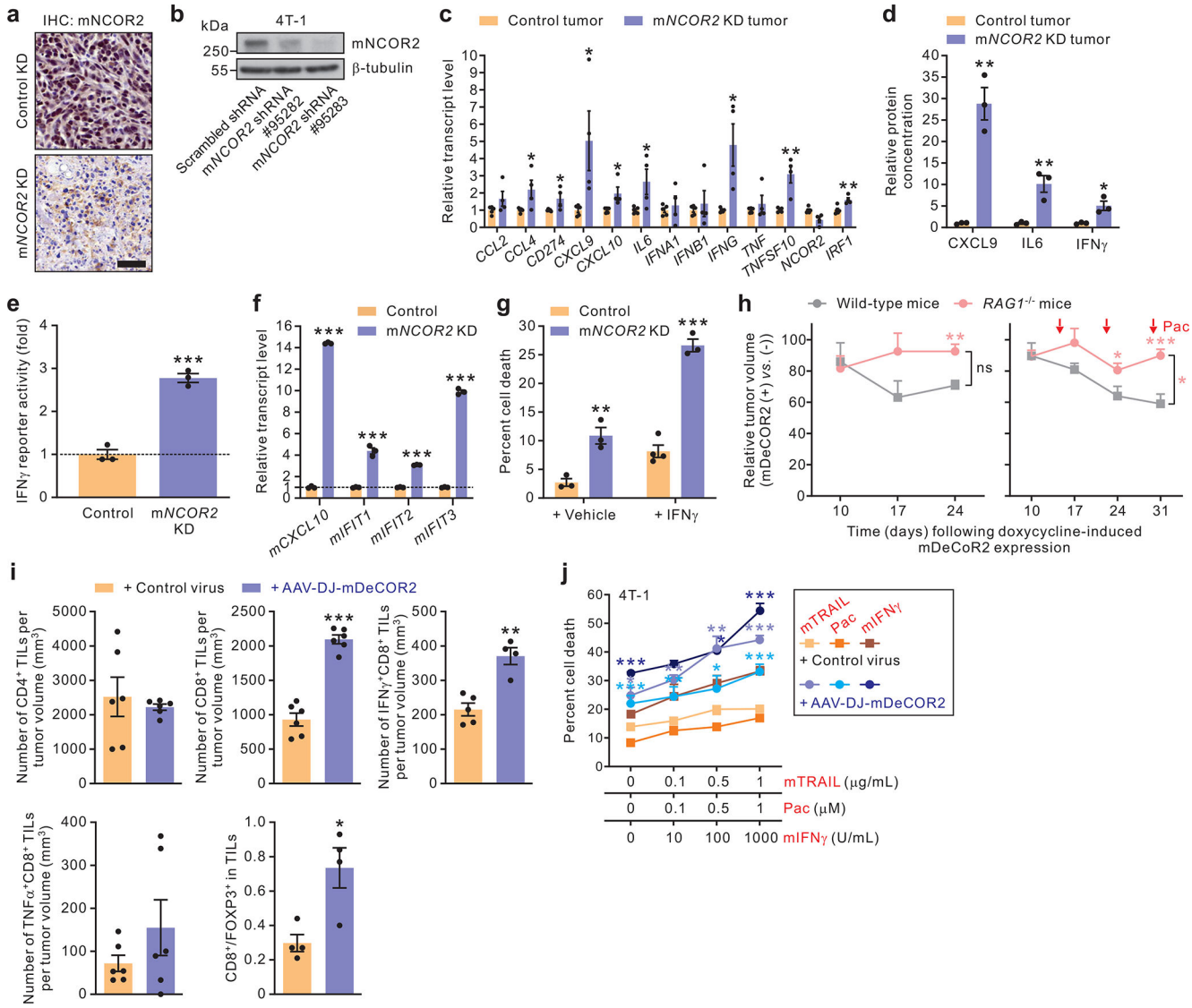

Fig. 7 |. NCOR2 deficiency or its functional inhibition creates a T-cell-inflamed tumor microenvironment.

a, IHC staining of murine NCOR2 (mNCOR2) in 4T-1 syngeneic orthotopic tumor. The tumor established by 4T-1 cells with KD of m*NCOR2* expression was included as a control (representative data of n=5 tumors with similar results). Scale bar, 25 μm. **b,** KD of m*NCOR2* expression in 4T-1 murine mammary tumor cells using lentivirus-mediated transduction of shRNAs (representative data of n=2 independent experiments with similar results). **c,** The transcript levels of antitumor immune regulatory genes expressed in the 4T-1 murine syngeneic breast cancer tumors with KD of m*NCOR2* or with scrambled shRNA (control). Data are presented as mean ± s.e.m.; n=4–5 tumors per group, the exact n are provided in the numerical source data). **d,** The amounts of CXCL9, IL6, and IFNγ in the protein lysates of the tumors described in **c**. **e,f,** The impact of m*NCOR2* KD on IFNγ reporter activity (**e**) and the transcript levels of the indicated IFNγ pathway genes (**f**) in 4T1 cells treated with IFNγ (1000 unit/ml × 16 hr) or vehicle (n=3 independent experiments). **g,** 4T1 cells with KD of m*NCOR2* expression were more sensitive to IFN-γ treatments

(*n*=3–4 independent experiments, the exact *n* are provided in the numerical source data). **h,** The average tumor volumes in the syngeneic 4T-1/BALB/c tumor model in wide-type mice *versus* in the same tumor model established in $RAG1^{-/-}$ mice following doxycycline-induced expression of murine DeCOR2 (mDeCOR2) and treated with paclitaxel (Pac) or vehicle (*n*=7–8 tumors per group, the exact *n* are provided in the numerical source data). **i,** The number of $CD4^+$ TILs ($CD45^+$), $CD8^+$ TILs, IFN-γ^+ and TNF-α^+ cells in the isolated $CD8^+$ TILs and the ratio of $CD8^+$ T-effector cells to $FoxP3^+$ T-regulatory cells (*n* = 4–6 tumors per group, the exact *n* are provided in the numerical source data). **j,** 4T-1 cells infected with AAV-DJ-mNCOR2 were more sensitive to murine TRAIL (mTRAIL), Pac, or murine IFN-γ (mIFN-γ) (*n*=2–7 independent experiments, the exact *n* are provided in the numerical source data). Data are represented as mean ± s.e.m. (**c**-**j**). **P* < 0.05; ***P* < 0.01; ****P* < 0.001 compared to control tumor (**c**,**d**), scrambled shRNA (control; **e**-**g**), wild-type mice (**h**), or control virus (**i**,**j**), two-tailed unpaired Student's *t*-test, or ordinary two-way ANOVA (**h**).

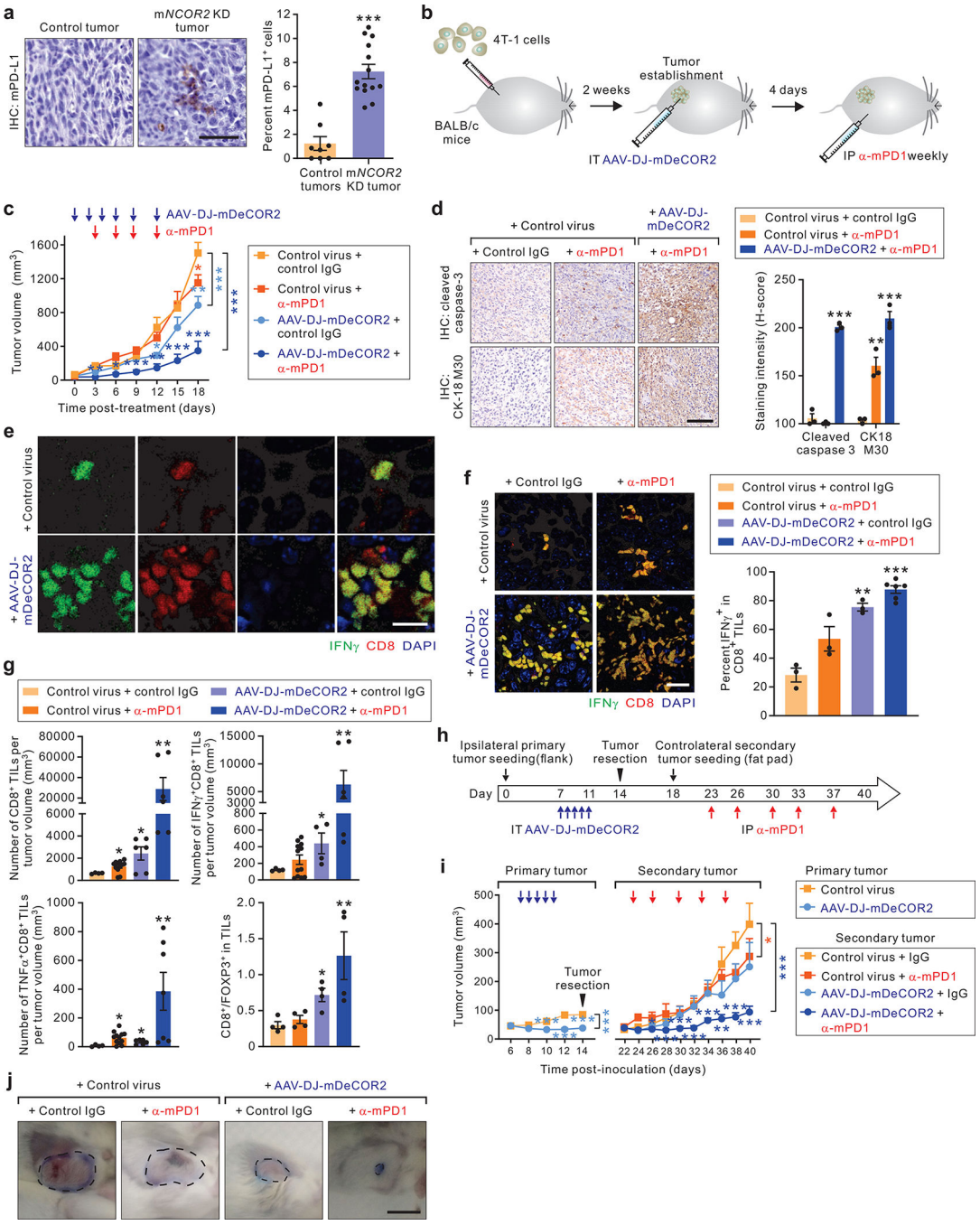

Fig. 8 |. Functional blocking of NCOR2 potentiates immune checkpoint therapy.

a, IHC images of murine programmed death ligand 1 (mPD-L1) in syngeneic orthotopic tumors established by 4T-1 cells with KD of murine *NCOR2* (m*NCOR2*) or those transduced with a control-shRNA (control). Scale bar, 50 μm. Right: The percentage of mPDL1-expressing (≥ 2+) cells in the tumors. Data are presented as mean ± s.e.m.; n=8–14 tumors (the exact n are provided in the numerical source data). **b**, The AAV-DJ-mDeCOR2/ anti-programmed cell death-1 (mPD1) combo therapy in the orthotopic and syngeneic mouse model of breast cancer (Methods). **c**, The changes in tumor volume with and without

treatment as described in **b** (n=10 mice per group). **d**, IHC staining of cleaved caspase 3 and CK18 M30 in the tumor tissues as treated in **b**. Scale bar, 100 μm. Right: The staining intensity of the indicated markers (n=3 tumors per group). **e**, The syngeneic 4T-1 tumors treated with AAV-DJ-mDeCOR2 or the control virus were immunostained with anti-IFN-γ or anti-CD8. Scale bar, 10 μm. **f**, Immunofluorescence images of the 4T-1 tumors treated as in **b** immunostained as in **e**. Scale bar, 20 μm. Right: The percentage of IFN-γ^+ cells in $CD8^+$ TILs in the treated tumors (n=3 tumors per group). **g**, The number of $CD4^+$ TILs, $CD8^+$ TILs, IFN-γ and TNF-α expression in the isolated $CD8^+$ TILs, and the ratio of $CD8^+$ T-effector cells to $FoxP3^+$ T-regulatory cells in the tumors treated in **b** (n=3–12 tumors per group, the exact n are provided in the numerical source data). **h**, The schedule used for the tumor rechallenge and AAV-DJ-mDeCOR2 neoadjuvant therapy model. **i**, The changes in the volume of primary and secondary tumors with and without treatment as in **h** (n=4–9 mice per group, the exact n are provided in the numerical source data). **j**, Representative pictures of the secondary tumors upon completion of the treatments as described in **i**. Scale bar, 10 mm. Data are represented as mean ± s.e.m. (**a**,**c**,**d**,**f**,**g**,**i**). *P < 0.05; **P < 0.01; ***P < 0.001 compared to control virus *plus* control IgG (**c**,**d**,**f**,**g**,**i**), two-tailed unpaired Student's t-test, or ordinary two-way ANOVA (**c**,**i**).